38. KINEMATICS

Revised January 2000 by J.D. Jackson (LBNL).

Throughout this section units are used in which $\hbar = c = 1$. The following conversions are useful: $\hbar c = 197.3$ MeV fm, $(\hbar c)^2 = 0.3894$ (GeV)^2 mb.

38.1. Lorentz transformations

The energy E and 3-momentum $\boldsymbol{p}$ of a particle of mass m form a 4-vector $p = (E, \boldsymbol{p})$ whose square $p^2 \equiv E^2 - |\boldsymbol{p}|^2 = m^2$. The velocity of the particle is $\boldsymbol{\beta} = \boldsymbol{p}/E$. The energy and momentum $(E^*, \boldsymbol{p}^*)$ viewed from a frame moving with velocity $\boldsymbol{\beta}_f$ are given by

$$\begin{pmatrix} E^* \\ p^*_\parallel \end{pmatrix} = \begin{pmatrix} \gamma_f & -\gamma_f\beta_f \\ -\gamma_f\beta_f & \gamma_f \end{pmatrix} \begin{pmatrix} E \\ p_\parallel \end{pmatrix} \ , \quad p^*_T = p_T \ , \tag{38.1}$$

where $\gamma_f = (1 - \beta_f^2)^{-1/2}$ and p_T ($p_\parallel$) are the components of $\boldsymbol{p}$ perpendicular (parallel) to $\boldsymbol{\beta}_f$. Other 4-vectors, such as the space-time coordinates of events, of course transform in the same way. The scalar product of two 4-momenta $p_1 \cdot p_2 = E_1 E_2 - \boldsymbol{p}_1 \cdot \boldsymbol{p}_2$ is invariant (frame independent).

38.2. Center-of-mass energy and momentum

In the collision of two particles of masses m_1 and m_2 the total center-of-mass energy can be expressed in the Lorentz-invariant form

$$\begin{aligned} E_{\rm cm} &= \Big[(E_1 + E_2)^2 - (\boldsymbol{p}_1 + \boldsymbol{p}_2)^2\Big]^{1/2} \ , \\ &= \Big[m_1^2 + m_2^2 + 2E_1E_2(1 - \beta_1\beta_2\cos\theta)\Big]^{1/2} \ , \end{aligned} \tag{38.2}$$

where θ is the angle between the particles. In the frame where one particle (of mass m_2) is at rest (lab frame),

$$E_{\rm cm} = (m_1^2 + m_2^2 + 2E_{1\,\rm lab}\, m_2)^{1/2} \ . \tag{38.3}$$

The velocity of the center-of-mass in the lab frame is

$$\boldsymbol{\beta}_{\rm cm} = \boldsymbol{p}_{\rm lab}/(E_{1\,\rm lab} + m_2) \ , \tag{38.4}$$

where $\boldsymbol{p}_{\rm lab} \equiv \boldsymbol{p}_{1\,\rm lab}$ and

$$\gamma_{\rm cm} = (E_{1\,\rm lab} + m_2)/E_{\rm cm} \ . \tag{38.5}$$

The c.m. momenta of particles 1 and 2 are of magnitude

$$p_{\rm cm} = p_{\rm lab}\frac{m_2}{E_{\rm cm}} \ . \tag{38.6}$$

For example, if a 0.80 GeV/c kaon beam is incident on a proton target, the center of mass energy is 1.699 GeV and the center of mass momentum of either particle is 0.442 GeV/c. It is also useful to note that

$$E_{\rm cm}\, dE_{\rm cm} = m_2\, dE_{1\,\rm lab} = m_2\, \beta_{1\,\rm lab}\, dp_{\rm lab} \ . \tag{38.7}$$

38.3. Lorentz-invariant amplitudes

The matrix elements for a scattering or decay process are written in terms of an invariant amplitude $-i\mathscr{M}$. As an example, the S-matrix for $2 \to 2$ scattering is related to $\mathscr{M}$ by

$$\begin{aligned} \langle p_1' p_2' \, |S| \, p_1 p_2 \rangle &= I - i(2\pi)^4\, \delta^4(p_1 + p_2 - p_1' - p_2') \\ &\times \frac{\mathscr{M}(p_1,\, p_2;\, p_1',\, p_2')}{(2E_1)^{1/2}\,(2E_2)^{1/2}\,(2E_1')^{1/2}\,(2E_2')^{1/2}} \ . \end{aligned} \tag{38.8}$$

The state normalization is such that

$$\langle p' | p \rangle = (2\pi)^3 \delta^3(\boldsymbol{p} - \boldsymbol{p}') \ . \tag{38.9}$$

38.4. Particle decays

The partial decay rate of a particle of mass M into n bodies in its rest frame is given in terms of the Lorentz-invariant matrix element $\mathscr{M}$ by

$$d\Gamma = \frac{(2\pi)^4}{2M}\, |\mathscr{M}|^2\, d\Phi_n\, (P;\, p_1, \ldots, p_n), \tag{38.10}$$

where $d\Phi_n$ is an element of n-body phase space given by

$$d\Phi_n(P;\, p_1, \ldots, p_n) = \delta^4\, (P - \sum_{i=1}^{n} p_i) \prod_{i=1}^{n} \frac{d^3 p_i}{(2\pi)^3 2E_i} \ . \tag{38.11}$$

This phase space can be generated recursively, viz.

$$\begin{aligned} d\Phi_n(P;\, p_1, \ldots, p_n) &= d\Phi_j(q;\, p_1, \ldots, p_j) \\ &\times\ d\Phi_{n-j+1}\, (P;\, q,\, p_{j+1}, \ldots, p_n)(2\pi)^3 dq^2 \ , \end{aligned} \tag{38.12}$$

where $q^2 = (\sum_{i=1}^{j} E_i)^2 - \Big|\sum_{i=1}^{j} \boldsymbol{p}_i\Big|^2$. This form is particularly useful in the case where a particle decays into another particle that subsequently decays.

38.4.1. *Survival probability*:

If a particle of mass M has mean proper lifetime τ ($= 1/\Gamma$) and has momentum $(E, \boldsymbol{p})$, then the probability that it lives for a time t_0 or greater before decaying is given by

$$P(t_0) = e^{-t_0\, \Gamma/\gamma} = e^{-Mt_0\, \Gamma/E} \ , \tag{38.13}$$

and the probability that it travels a distance x_0 or greater is

$$P(x_0) = e^{-Mx_0\, \Gamma/|\boldsymbol{p}|} \ . \tag{38.14}$$

38.4.2. *Two-body decays*:

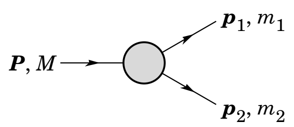

Figure 38.1: Definitions of variables for two-body decays.

In the rest frame of a particle of mass M, decaying into 2 particles labeled 1 and 2,

$$E_1 = \frac{M^2 - m_2^2 + m_1^2}{2M} \ , \tag{38.15}$$

$$\begin{aligned} |\boldsymbol{p}_1| &= |\boldsymbol{p}_2| \\ &= \frac{\Big[\big(M^2 - (m_1 + m_2)^2\big)\big(M^2 - (m_1 - m_2)^2\big)\Big]^{1/2}}{2M} \ , \end{aligned} \tag{38.16}$$

and

$$d\Gamma = \frac{1}{32\pi^2}\, |\mathscr{M}|^2\, \frac{|\boldsymbol{p}_1|}{M^2}\, d\Omega \ , \tag{38.17}$$

where $d\Omega = d\phi_1 d(\cos\theta_1)$ is the solid angle of particle 1.

38.4.3. *Three-body decays*:

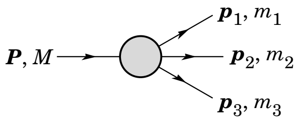

Figure 38.2: Definitions of variables for three-body decays.

Defining $p_{ij} = p_i + p_j$ and $m_{ij}^2 = p_{ij}^2$, then $m_{12}^2 + m_{23}^2 + m_{13}^2 = M^2 + m_1^2 + m_2^2 + m_3^2$ and $m_{12}^2 = (P - p_3)^2 = M^2 + m_3^2 - 2ME_3$, where E_3 is the energy of particle 3 in the rest frame of M. In that frame, the momenta of the three decay particles lie in a plane. The relative orientation of these three momenta is fixed if their energies are known. The momenta can therefore be specified in space by giving three Euler angles (α, β, γ) that specify the orientation of the final system relative to the initial particle [1]. Then

$$d\Gamma = \frac{1}{(2\pi)^5} \frac{1}{16M} \, |\mathscr{M}|^2 \, dE_1 \, dE_2 \, d\alpha \, d(\cos\beta) \, d\gamma \; . \tag{38.18}$$

Alternatively

$$d\Gamma = \frac{1}{(2\pi)^5} \frac{1}{16M^2} \, |\mathscr{M}|^2 \, |\boldsymbol{p}_1^*| \, |\boldsymbol{p}_3| \, dm_{12} \, d\Omega_1^* \, d\Omega_3 \; , \tag{38.19}$$

where $(|\boldsymbol{p}_1^*|, \, \Omega_1^*)$ is the momentum of particle 1 in the rest frame of 1 and 2, and Ω_3 is the angle of particle 3 in the rest frame of the decaying particle. $|\boldsymbol{p}_1^*|$ and $|\boldsymbol{p}_3|$ are given by

$$|\boldsymbol{p}_1^*| = \frac{\left[\left(m_{12}^2 - (m_1 + m_2)^2\right)\left(m_{12}^2 - (m_1 - m_2)^2\right)\right]^{1/2}}{2m_{12}} \; , \tag{38.20a}$$

and

$$|\boldsymbol{p}_3| = \frac{\left[\left(M^2 - (m_{12} + m_3)^2\right)\left(M^2 - (m_{12} - m_3)^2\right)\right]^{1/2}}{2M} \; . \tag{38.20b}$$

[Compare with Eq. (38.16).]

If the decaying particle is a scalar or we average over its spin states, then integration over the angles in Eq. (38.18) gives

$$\begin{aligned} d\Gamma &= \frac{1}{(2\pi)^3} \frac{1}{8M} \, \overline{|\mathscr{M}|^2} \, dE_1 \, dE_2 \\ &= \frac{1}{(2\pi)^3} \frac{1}{32M^3} \, \overline{|\mathscr{M}|^2} \, dm_{12}^2 \, dm_{23}^2 \; . \end{aligned} \tag{38.21}$$

This is the standard form for the Dalitz plot.

38.4.3.1. *Dalitz plot:* For a given value of m_{12}^2, the range of m_{23}^2 is determined by its values when $\boldsymbol{p}_2$ is parallel or antiparallel to $\boldsymbol{p}_3$:

$$(m_{23}^2)_{\max} = (E_2^* + E_3^*)^2 - \left(\sqrt{E_2^{*2} - m_2^2} - \sqrt{E_3^{*2} - m_3^2}\right)^2 \; , \tag{38.22a}$$

$$(m_{23}^2)_{\min} = (E_2^* + E_3^*)^2 - \left(\sqrt{E_2^{*2} - m_2^2} + \sqrt{E_3^{*2} - m_3^2}\right)^2 \; . \tag{38.22b}$$

Here $E_2^* = (m_{12}^2 - m_1^2 + m_2^2)/2m_{12}$ and $E_3^* = (M^2 - m_{12}^2 - m_3^2)/2m_{12}$ are the energies of particles 2 and 3 in the m_{12} rest frame. The scatter plot in m_{12}^2 and m_{23}^2 is called a Dalitz plot. If $\overline{|\mathscr{M}|^2}$ is constant, the allowed region of the plot will be uniformly populated with events [see Eq. (38.21)]. A nonuniformity in the plot gives immediate information on $|\mathscr{M}|^2$. For example, in the case of $D \to K\pi\pi$, bands appear when $m_{(K\pi)} = m_{K^*(892)}$, reflecting the appearance of the decay chain $D \to K^*(892)\pi \to K\pi\pi$.

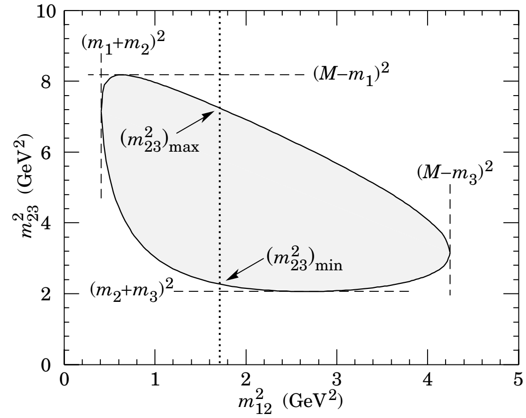

Figure 38.3: Dalitz plot for a three-body final state. In this example, the state is $\pi^+ \overline{K}^0 p$ at 3 GeV. Four-momentum conservation restricts events to the shaded region.

38.4.4. ***Kinematic limits***: In a three-body decay the maximum of $|\boldsymbol{p}_3|$, [given by Eq. (38.20)], is achieved when $m_{12} = m_1 + m_2$, *i.e.*, particles 1 and 2 have the same vector velocity in the rest frame of the decaying particle. If, in addition, $m_3 > m_1, m_2$, then $|\boldsymbol{p}_3|_{\max} > |\boldsymbol{p}_1|_{\max}, \, |\boldsymbol{p}_2|_{\max}$.

38.4.5. ***Multibody decays***: The above results may be generalized to final states containing any number of particles by combining some of the particles into "effective particles" and treating the final states as 2 or 3 "effective particle" states. Thus, if $p_{ijk\ldots} = p_i + p_j + p_k + \ldots$, then

$$m_{ijk\ldots} = \sqrt{p^2{}_{ijk\ldots}} \; , \tag{38.23}$$

and $m_{ijk\ldots}$ may be used in place of *e.g.*, m_{12} in the relations in Sec. 38.4.3 or 38.4.3.1 above.

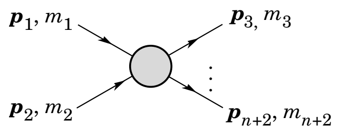

Figure 38.4: Definitions of variables for production of an n-body final state.

38.5. Cross sections

The differential cross section is given by

$$d\sigma = \frac{(2\pi)^4 |\mathscr{M}|^2}{4\sqrt{(p_1 \cdot p_2)^2 - m_1^2 m_2^2}} \times d\Phi_n(p_1 + p_2; \, p_3, \, \ldots, \, p_{n+2}) \; . \tag{38.24}$$

[See Eq. (38.11).] In the rest frame of m_2(lab),

$$\sqrt{(p_1 \cdot p_2)^2 - m_1^2 m_2^2} = m_2 p_{1\,\text{lab}} \; ; \tag{38.25a}$$

while in the center-of-mass frame

$$\sqrt{(p_1 \cdot p_2)^2 - m_1^2 m_2^2} = p_{1\text{cm}} \sqrt{s} \; . \tag{38.25b}$$

38.5.1. *Two-body reactions*:

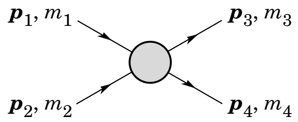

Figure 38.5: Definitions of variables for a two-body final state.

Two particles of momenta p_1 and p_2 and masses m_1 and m_2 scatter to particles of momenta p_3 and p_4 and masses m_3 and m_4; the Lorentz-invariant Mandelstam variables are defined by

$$\begin{aligned} s &= (p_1+p_2)^2 = (p_3+p_4)^2 \\ &= m_1^2 + 2E_1E_2 - 2\boldsymbol{p}_1\cdot\boldsymbol{p}_2 + m_2^2\ , \qquad (38.26) \\ t &= (p_1-p_3)^2 = (p_2-p_4)^2 \\ &= m_1^2 - 2E_1E_3 + 2\boldsymbol{p}_1\cdot\boldsymbol{p}_3 + m_3^2\ , \qquad (38.27) \\ u &= (p_1-p_4)^2 = (p_2-p_3)^2 \\ &= m_1^2 - 2E_1E_4 + 2\boldsymbol{p}_1\cdot\boldsymbol{p}_4 + m_4^2\ , \qquad (38.28) \end{aligned}$$

and they satisfy

$$s + t + u = m_1^2 + m_2^2 + m_3^2 + m_4^2\ . \qquad (38.29)$$

The two-body cross section may be written as

$$\frac{d\sigma}{dt} = \frac{1}{64\pi s}\frac{1}{|\boldsymbol{p}_{1\text{cm}}|^2}|\mathscr{M}|^2\ . \qquad (38.30)$$

In the center-of-mass frame

$$\begin{aligned} t &= (E_{1\text{cm}} - E_{3\text{cm}})^2 - (p_{1\text{cm}} - p_{3\text{cm}})^2 - 4p_{1\text{cm}}\,p_{3\text{cm}}\,\sin^2(\theta_{\text{cm}}/2) \\ &= t_0 - 4p_{1\text{cm}}\,p_{3\text{cm}}\,\sin^2(\theta_{\text{cm}}/2)\ , \qquad (38.31) \end{aligned}$$

where θ_{cm} is the angle between particle 1 and 3. The limiting values t_0 ($\theta_{\text{cm}} = 0$) and t_1 ($\theta_{\text{cm}} = \pi$) for $2 \to 2$ scattering are

$$t_0(t_1) = \left[\frac{m_1^2 - m_3^2 - m_2^2 + m_4^2}{2\sqrt{s}}\right]^2 - (p_{1\,\text{cm}} \mp p_{3\,\text{cm}})^2\ . \qquad (38.32)$$

In the literature the notation $t_{\min}$ ($t_{\max}$) for t_0 (t_1) is sometimes used, which should be discouraged since $t_0 > t_1$. The center-of-mass energies and momenta of the incoming particles are

$$E_{1\text{cm}} = \frac{s + m_1^2 - m_2^2}{2\sqrt{s}}\ , \qquad E_{2\text{cm}} = \frac{s + m_2^2 - m_1^2}{2\sqrt{s}}\ , \qquad (38.33)$$

For $E_{3\text{cm}}$ and $E_{4\text{cm}}$, change m_1 to m_3 and m_2 to m_4. Then

$$p_{i\,\text{cm}} = \sqrt{E_{i\,\text{cm}}^2 - m_i^2} \text{ and } p_{1\text{cm}} = \frac{p_{1\,\text{lab}}\,m_2}{\sqrt{s}}\ . \qquad (38.34)$$

Here the subscript lab refers to the frame where particle 2 is at rest. [For other relations see Eqs. (38.2)–(38.4).]

38.5.2. *Inclusive reactions*:

Choose some direction (usually the beam direction) for the z-axis; then the energy and momentum of a particle can be written as

$$E = m_T\cosh y\ ,\ p_x\ ,\ p_y\ ,\ p_z = m_T\sinh y\ , \qquad (38.35)$$

where m_T is the transverse mass

$$m_T^2 = m^2 + p_x^2 + p_y^2\ , \qquad (38.36)$$

and the rapidity y is defined by

$$\begin{aligned} y &= \frac{1}{2}\ln\left(\frac{E+p_z}{E-p_z}\right) \\ &= \ln\left(\frac{E+p_z}{m_T}\right) = \tanh^{-1}\left(\frac{p_z}{E}\right)\ . \qquad (38.37) \end{aligned}$$

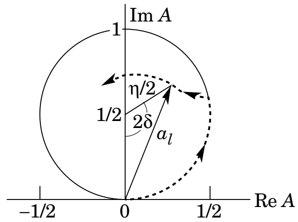

Figure 38.6: Argand plot showing a partial-wave amplitude a_ℓ as a function of energy. The amplitude leaves the unitary circle where inelasticity sets in ($\eta_\ell < 1$).

Under a boost in the z-direction to a frame with velocity β, $y \to y - \tanh^{-1}\beta$. Hence the shape of the rapidity distribution dN/dy is invariant. The invariant cross section may also be rewritten

$$E\frac{d^3\sigma}{d^3p} = \frac{d^3\sigma}{d\phi\,dy\,p_T\,dp_T} \Longrightarrow \frac{d^2\sigma}{\pi\,dy\,d(p_T^2)}\ . \qquad (38.38)$$

The second form is obtained using the identity $dy/dp_z = 1/E$, and the third form represents the average over ϕ.

Feynman's x variable is given by

$$x = \frac{p_z}{p_{z\,\max}} \approx \frac{E+p_z}{(E+p_z)_{\max}} \quad (p_T \ll |p_z|)\ . \qquad (38.39)$$

In the c.m. frame,

$$x \approx \frac{2p_{z\,\text{cm}}}{\sqrt{s}} = \frac{2m_T\sinh y_{\text{cm}}}{\sqrt{s}} \qquad (38.40)$$

and

$$= (y_{\text{cm}})_{\max} = \ln(\sqrt{s}/m)\ . \qquad (38.41)$$

For $p \gg m$, the rapidity [Eq. (38.37)] may be expanded to obtain

$$\begin{aligned} y &= \frac{1}{2}\ln\frac{\cos^2(\theta/2) + m^2/4p^2 + \ldots}{\sin^2(\theta/2) + m^2/4p^2 + \ldots} \\ &\approx -\ln\tan(\theta/2) \equiv \eta \qquad (38.42) \end{aligned}$$

where $\cos\theta = p_z/p$. The pseudorapidity η defined by the second line is approximately equal to the rapidity y for $p \gg m$ and $\theta \gg 1/\gamma$, and in any case can be measured when the mass and momentum of the particle is unknown. From the definition one can obtain the identities

$$\sinh\eta = \cot\theta\ ,\quad \cosh\eta = 1/\sin\theta\ ,\quad \tanh\eta = \cos\theta\ . \qquad (38.43)$$

38.5.3. *Partial waves*:

The amplitude in the center of mass for elastic scattering of spinless particles may be expanded in Legendre polynomials

$$f(k,\theta) = \frac{1}{k}\sum_\ell (2\ell+1)a_\ell P_\ell(\cos\theta)\ , \qquad (38.44)$$

where k is the c.m. momentum, θ is the c.m. scattering angle, $a_\ell = (\eta_\ell e^{2i\delta_\ell} - 1)/2i$, $0 \le \eta_\ell \le 1$, and δ_ℓ is the phase shift of the ℓ^{th} partial wave. For purely elastic scattering, $\eta_\ell = 1$. The differential cross section is

$$\frac{d\sigma}{d\Omega} = |f(k,\theta)|^2\ . \qquad (38.45)$$

The optical theorem states that

$$\sigma_{\text{tot}} = \frac{4\pi}{k}\text{Im}\,f(k,0)\ , \qquad (38.46)$$

and the cross section in the ℓ^{th} partial wave is therefore bounded:

$$\sigma_\ell = \frac{4\pi}{k^2}(2\ell+1)|a_\ell|^2 \le \frac{4\pi(2\ell+1)}{k^2}\ . \qquad (38.47)$$

The evolution with energy of a partial-wave amplitude a_ℓ can be displayed as a trajectory in an Argand plot, as shown in Fig. 38.6.

The usual Lorentz-invariant matrix element $\mathscr{M}$ (see Sec. 38.3 above) for the elastic process is related to $f(k,\theta)$ by

$$\mathscr{M} = -8\pi\sqrt{s}\, f(k,\theta) \ , \tag{38.48}$$

so

$$\sigma_{\rm tot} = -\frac{1}{2p_{\rm lab}\, m_2}\, {\rm Im}\, \mathscr{M}(t=0) \ , \tag{38.49}$$

where s and t are the center-of-mass energy squared and momentum transfer squared, respectively (see Sec. 38.4.1).

38.5.3.1. *Resonances:* The Breit-Wigner (nonrelativistic) form for an elastic amplitude a_ℓ with a resonance at c.m. energy E_R, elastic width $\Gamma_{\rm el}$, and total width $\Gamma_{\rm tot}$ is

$$a_\ell = \frac{\Gamma_{\rm el}/2}{E_R - E - i\Gamma_{\rm tot}/2} \ , \tag{38.50}$$

where E is the c.m. energy. As shown in Fig. 38.7, in the absence of background the elastic amplitude traces a counterclockwise circle with center $ix_{\rm el}/2$ and radius $x_{\rm el}/2$, where the elasticity $x_{\rm el} = \Gamma_{\rm el}/\Gamma_{\rm tot}$. The amplitude has a pole at $E = E_R - i\Gamma_{\rm tot}/2$.

The spin-averaged Breit-Wigner cross section for a spin-J resonance produced in the collision of particles of spin S_1 and S_2 is

$$\sigma_{BW}(E) = \frac{(2J+1)}{(2S_1+1)(2S_2+1)}\,\frac{\pi}{k^2}\,\frac{B_{\rm in}B_{\rm out}\Gamma^2_{\rm tot}}{(E-E_R)^2 + \Gamma^2_{\rm tot}/4} \ , \tag{38.51}$$

where k is the c.m. momentum, E is the c.m. energy, and $B_{\rm in}$ and $B_{\rm out}$ are the branching fractions of the resonance into the entrance and exit channels. The $2S+1$ factors are the multiplicities of the incident spin states, and are replaced by 2 for photons. This expression is valid only for an isolated state. If the width is not small, $\Gamma_{\rm tot}$ cannot be treated as a constant independent of E. There are many other forms for σ_{BW}, all of which are equivalent to the one given here in the narrow-width case. Some of these forms may be more appropriate if the resonance is broad.

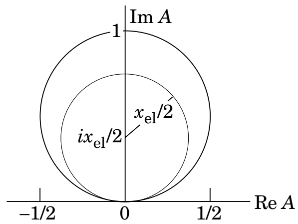

Figure 38.7: Argand plot for a resonance.

The relativistic Breit-Wigner form corresponding to Eq. (38.50) is:

$$a_\ell = \frac{-m\Gamma_{\rm el}}{s - m^2 + im\Gamma_{\rm tot}} \ . \tag{38.52}$$

A better form incorporates the known kinematic dependences, replacing $m\Gamma_{\rm tot}$ by $\sqrt{s}\,\Gamma_{\rm tot}(s)$, where $\Gamma_{\rm tot}(s)$ is the width the resonance particle would have if its mass were $\sqrt{s}$, and correspondingly $m\Gamma_{\rm el}$ by $\sqrt{s}\,\Gamma_{\rm el}(s)$ where $\Gamma_{\rm el}(s)$ is the partial width in the incident channel for a mass $\sqrt{s}$:

$$a_\ell = \frac{-\sqrt{s}\,\Gamma_{\rm el}(s)}{s - m^2 + i\sqrt{s}\,\Gamma_{\rm tot}(s)} \ . \tag{38.53}$$

For the Z boson, all the decays are to particles whose masses are small enough to be ignored, so on dimensional grounds $\Gamma_{\rm tot}(s) = \sqrt{s}\,\Gamma_0/m_Z$, where Γ_0 defines the width of the Z, and $\Gamma_{\rm el}(s)/\Gamma_{\rm tot}(s)$ is constant. A full treatment of the line shape requires consideration of dynamics, not just kinematics. For the Z this is done by calculating the radiative corrections in the Standard Model.

References:

1. See, for example, J.J. Sakurai, *Modern Quantum Mechnaics*, Addison-Wesley (1985), p. 172, or D.M. Brink and G.R. Satchler, *Angular Momentum*, 2nd ed., Oxford University Press (1968), p. 20.

39. CROSS-SECTION FORMULAE FOR SPECIFIC PROCESSES

Revised October 2001 by R.N. Cahn (LBNL).

39.1. Leptoproduction

See section on Structure Functions (Sec. 16 of this *Review*).

39.2. e^+e^- annihilation

For pointlike, spin-1/2 fermions, the differential cross section in the c.m. for $e^+e^- \to f\overline{f}$ via single photon annihilation is (θ is the angle between the incident electron and the produced fermion; $N_c = 1$ if f is a lepton and $N_c = 3$ if f is a quark).

$$\frac{d\sigma}{d\Omega} = N_c \frac{\alpha^2}{4s} \beta \left[1 + \cos^2\theta + (1-\beta^2)\sin^2\theta\right] Q_f^2 \;, \tag{39.1}$$

where β is the velocity of the final state fermion in the c.m. and Q_f is the charge of the fermion in units of the proton charge. For $\beta \to 1$,

$$\sigma = N_c \frac{4\pi\alpha^2}{3s} Q_f^2 = N_c \frac{86.8 Q_f^2 \; nb}{s} \;. \tag{39.2}$$

where s is in GeV^2 units.

At higher energies, the Z^0 (mass M_Z and width Γ_Z) must be included. If the mass of a fermion f is much less than the mass of the Z^0, then the differential cross section for $e^+e^- \to f\overline{f}$ is

$$\begin{aligned}\frac{d\sigma}{d\Omega} = \; & N_c \frac{\alpha^2}{4s} \Big\{ (1+\cos^2\theta) \left[Q_f^2 - 2\chi_1 v_e v_f Q_f + \chi_2 (a_e^2 + v_e^2)(a_f^2 + v_f^2) \right] \\ & + 2\cos\theta \left[-2\chi_1 a_e a_f Q_f + 4\chi_2 a_e a_f v_e v_f \right] \Big\}\end{aligned} \tag{39.3}$$

where

$$\begin{aligned}\chi_1 &= \frac{1}{16\sin^2\theta_W \cos^2\theta_W} \frac{s(s-M_Z^2)}{(s-M_Z^2)^2 + M_Z^2\Gamma_Z^2} \;, \\ \chi_2 &= \frac{1}{256\sin^4\theta_W \cos^4\theta_W} \frac{s^2}{(s-M_Z^2)^2 + M_Z^2\Gamma_Z^2} \;, \\ a_e &= -1 \;, \\ v_e &= -1 + 4\sin^2\theta_W \;, \\ a_f &= 2T_{3f} \;, \\ v_f &= 2T_{3f} - 4Q_f \sin^2\theta_W \;,\end{aligned} \tag{39.4}$$

where $T_{3f} = 1/2$ for u, c and neutrinos, while $T_{3f} = -1/2$ for d, s, b, and negatively charged leptons.

At LEP II it may be possible to produce the orthodox Higgs boson, H, (see the mini-review on Higgs bosons) in the reaction $e^+e^- \to HZ^0$, which proceeds dominantly through a virtual Z^0. The Standard Model prediction for the cross section [3] is

$$\sigma(e^+e^- \to HZ^0) = \frac{\pi\alpha^2}{24} \cdot \frac{2K}{\sqrt{s}} \cdot \frac{K^2 + 3M_Z^2}{(s-M_Z^2)^2} \cdot \frac{1 - 4\sin^2\theta_W + 8\sin^4\theta_W}{\sin^4\theta_W \cos^4\theta_W} \;. \tag{39.5}$$

where K is the c.m. momentum of the produced H or Z^0. Near the production threshold, this formula needs to be corrected for the finite width of the Z^0.

39.3. Two-photon process at e^+e^- colliders

When an e^+ and an e^- collide with energies E_1 and E_2, they emit dn_1 and dn_2 virtual photons with energies ω_1 and ω_2 and 4-momenta q_1 and q_2. In the equivalent photon approximation, the cross section for $e^+e^- \to e^+e^-X$ is related to the cross section for $\gamma\gamma \to X$ by (Ref. 1)

$$d\sigma_{e^+e^- \to e^+e^- X}(s) = dn_1 \, dn_2 \, d\sigma_{\gamma\gamma \to X}(W^2) \tag{39.6}$$

where $s = 4E_1E_2$, $W^2 = 4\omega_1\omega_2$ and

$$dn_i = \frac{\alpha}{\pi} \left[1 - \frac{\omega_i}{E_i} + \frac{\omega_i^2}{2E_i^2} - \frac{m_e^2\omega_i^2}{(-q_i^2)E_i^2} \right] \frac{d\omega_i}{\omega_i} \frac{d(-q_i^2)}{(-q_i^2)} \;. \tag{39.7}$$

After integration (including that over q_i^2 in the region $m_e^2\omega_i^2/E_i(E_i - \omega_i) \le -q_i^2 \le (-q^2)_{\rm max}$), the cross section is

$$\begin{aligned}\sigma_{e^+e^- \to e^+e^- X}(s) = & \frac{\alpha^2}{\pi^2} \int_{z_{th}}^{1} \frac{dz}{z} \left[f(z) \left(\ln \frac{(-q^2)_{\rm max}}{m_e^2 z} - 1 \right)^2 \right. \\ & \left. - \tfrac{1}{3} \left(\ln \frac{1}{z} \right)^3 \right] \sigma_{\gamma\gamma \to X}(zs) \;; \\ f(z) = & \left(1 + \tfrac{1}{2}z\right)^2 \ln \frac{1}{z} - \tfrac{1}{2}(1-z)(3+z) \;; \\ z = & \frac{W^2}{s} \;.\end{aligned} \tag{39.8}$$

The quantity $(-q^2)_{\rm max}$ depends on properties of the produced system X, in particular, $(-q^2)_{\rm max} \sim m_\rho^2$ for hadron production ($X = h$) and $(-q^2)_{\rm max} \sim W^2$ for lepton pair production ($X = \ell^+\ell^-$, $\ell = e, \mu, \tau$).

For production of a resonance of mass m_R and spin $J \neq 1$

$$\begin{aligned}\sigma_{e^+e^- \to e^+e^- R}(s) = & (2J+1) \frac{8\alpha^2 \Gamma_{R \to \gamma\gamma}}{m_R^3} \\ & \times \left[f(m_R^2/s) \left(\ln \frac{s m_V^2}{m_e^2 m_R^2} - 1 \right)^2 - \frac{1}{3} \left(\ln \frac{s}{m_R^2} \right)^3 \right]\end{aligned} \tag{39.9}$$

where m_V is the mass that enters into the form factor of the $\gamma\gamma \to R$ transition: $m_V \sim m_\rho$ for $R = \pi^0$, η, $f_2(1270)$, …, $m_V \sim m_R$ for $R = c\overline{c}$ or $b\overline{b}$ resonances.

39.4. Inclusive hadronic reactions

One-particle inclusive cross sections $Ed^3\sigma/d^3p$ for the production of a particle of momentum p are conveniently expressed in terms of rapidity (see above) and the momentum p_T transverse to the beam direction (defined in the center-of-mass frame)

$$E \frac{d^3\sigma}{d^3p} = \frac{d^3\sigma}{d\phi \, dy \, p_T \, dp_T} \;. \tag{39.10}$$

In the case of processes where p_T is large or the mass of the produced particle is large (here large means greater than 10 GeV), the parton model can be used to calculate the rate. Symbolically

$$\sigma_{\rm hadronic} = \sum_{ij} \int f_i(x_1, Q^2) \, f_j(x_2, Q^2) \, dx_1 \, dx_2 \, \widehat{\sigma}_{\rm partonic} \;, \tag{39.11}$$

where $f_i(x, Q^2)$ is the parton distribution introduced above and Q is a typical momentum transfer in the partonic process and $\widehat{\sigma}$ is the partonic cross section. Some examples will help to clarify. The production of a W^+ in pp reactions at rapidity y in the center-of-mass frame is given by

$$\begin{aligned}\frac{d\sigma}{dy} = \frac{G_F \, \pi\sqrt{2}}{3} \times \tau \Big[& \cos^2\theta_c \Big(u(x_1, M_W^2) \, \overline{d}(x_2, M_W^2) \\ & + u(x_2, M_W^2) \, \overline{d}(x_1, M_W^2) \Big) \\ & + \sin^2\theta_c \Big(u(x_1, M_W^2) \, \overline{s}(x_2, M_W^2) \\ & + s(x_2, M_W^2) \, \overline{u}(x_1, M_W^2) \Big) \Big] \;,\end{aligned} \tag{39.12}$$

where $x_1 = \sqrt{\tau} \, e^{y}$, $x_2 = \sqrt{\tau} \, e^{-y}$, and $\tau = M_W^2/s$. Similarly the production of a jet in pp (or $p\overline{p}$) collisions is given by

$$\begin{aligned}\frac{d^3\sigma}{d^2p_T \, dy} = & \sum_{ij} \int f_i(x_1, p_T^2) \, f_j(x_2, p_T^2) \\ & \times \left[\widehat{s} \frac{d\widehat{\sigma}}{d\widehat{t}} \right]_{ij} dx_1 \, dx_2 \, \delta(\widehat{s} + \widehat{t} + \widehat{u}) \;,\end{aligned} \tag{39.13}$$

where the summation is over quarks, gluons, and antiquarks. Here

$$s = (p_1 + p_2)^2 \ , \tag{39.14}$$

$$t = (p_1 - p_{\rm jet})^2 \ , \tag{39.15}$$

$$u = (p_2 - p_{\rm jet})^2 \ , \tag{39.16}$$

p_1 and p_2 are the momenta of the incoming p and p (or $\overline{p}$) and $\widehat{s}$, $\widehat{t}$, and $\widehat{u}$ are s, t, and u with $p_1 \to x_1 p_1$ and $p_2 \to x_2 p_2$. The partonic cross section $\widehat{s}[(d\widehat{\sigma})/(d\widehat{t})]$ can be found in Ref. 2. Example: for the process $gg \to q\overline{q}$,

$$\widehat{s}\,\frac{d\sigma}{dt} = 3\alpha_s^2\,\frac{(\widehat{t}^{\,2} + \widehat{u}^2)}{8\widehat{s}}\left[\frac{4}{9\,\widehat{t}\,\widehat{u}} - \frac{1}{\widehat{s}^{\,2}}\right] . \tag{39.17}$$

The prediction of Eq. (39.13) is compared to data from the UA1 and UA2 collaborations in Fig. 40.1 in the Plots of Cross Sections and Related Quantities section of this *Review*.

The associated production of a Higgs boson and a gauge boson is analogous to the process $e^+e^- \to HZ^0$ in Sec. 39.2. The required parton-level cross sections [4], averaged over initial quark colors, are

$$\sigma(q_i\overline{q}_j \to W^\pm H) = \frac{\pi\alpha^2 |V_{ij}|^2}{36\sin^4\theta_W}\cdot\frac{2K}{\sqrt{s}}\cdot\frac{K^2 + 3M_W^2}{(s - M_W^2)^2}$$

$$\sigma(q\overline{q} \to Z^0 H) = \frac{\pi\alpha^2 (a_q^2 + v_q^2)}{144\sin^4\theta_W\cos^4\theta_W}\cdot\frac{2K}{\sqrt{s}}\cdot\frac{K^2 + 3M_Z^2}{(s - M_Z^2)^2} \ .$$

Here V_{ij} is the appropriate element of the Kobayashi-Maskawa matrix and K is the c.m. momentum of the produced H. The axial and vector couplings are defined as in Sec. 39.2.

39.5. One-particle inclusive distributions

In order to describe one-particle inclusive production in e^+e^- annihilation or deep inelastic scattering, it is convenient to introduce a fragmentation function $D_i^h\,(z, Q^2)$ where $D_i^h\,(z, Q^2)$ is the number of hadrons of type h and momentum between zp and $(z + dz)p$ produced in the fragmentation of a parton of type i. The Q^2 evolution is predicted by QCD and is similar to that of the parton distribution functions [see section on Quantum Chromodynamics (Sec. 9 of this *Review*)]. The $D_i^h(z, Q^2)$ are normalized so that

$$\sum_h \int z D_i^h\,(z, Q^2) dz = 1 \ . \tag{39.18}$$

If the contributions of the Z boson and three-jet events are neglected, the cross section for producing a hadron h in e^+e^- annihilation is given by

$$\frac{1}{\sigma_{\rm had}}\,\frac{d\sigma}{dz} = \frac{\sum_i e_i^2\, D_i^h\,(z, Q^2)}{\sum_i e_i^2} \ , \tag{39.19}$$

where e_i is the charge of quark-type i, $\sigma_{\rm had}$ is the total hadronic cross section, and the momentum of the hadron is $zE_{\rm cm}/2$.

In the case of deep inelastic muon scattering, the cross section for producing a hadron of energy E_h is given by

$$\frac{1}{\sigma_{\rm tot}}\,\frac{d\sigma}{dz} = \frac{\sum_i e_i^2\, q_i(x, Q^2)\, D_i^h(z, Q^2)}{\sum_i e_i^2\, q_i(x, Q^2)} \ , \tag{39.20}$$

where $E_h = \nu z$. (For the kinematics of deep inelastic scattering, see Sec. 38.4.2 of the Kinematics section of this *Review*.) The fragmentation functions for light and heavy quarks have a different z dependence; the former peak near $z = 0$. They are illustrated in Figs. 17.5a and 17.5b in the section on "Fragmentation Functions in e^+e^- Annihilation" (Sec. 17 of this *Review*).

References:

1. V.M. Budnev, I.F. Ginzburg, G.V. Meledin, and V.G. Serbo,Phys. Reports **15C**, 181 (1975);

   See also S. Brodsky, T. Kinoshita, and H. Terazawa, Phys. Rev. **D4**, 1532 (1971).
2. G.F. Owens, F. Reya, and M. Glück, Phys. Rev. **D18**, 1501 (1978).
3. B.W. Lee, C. Quigg, and B. Thacker, Phys. Rev. **D16**, 1519 (1977).
4. E. Eichten, I. Hinchliffe, K. Lane, and C. Quigg, Rev. Mod. Phys. **56**, 579 (1984).

40. PLOTS OF CROSS SECTIONS AND RELATED QUANTITIES

Jet Production in pp and $\overline{p}p$ Interactions

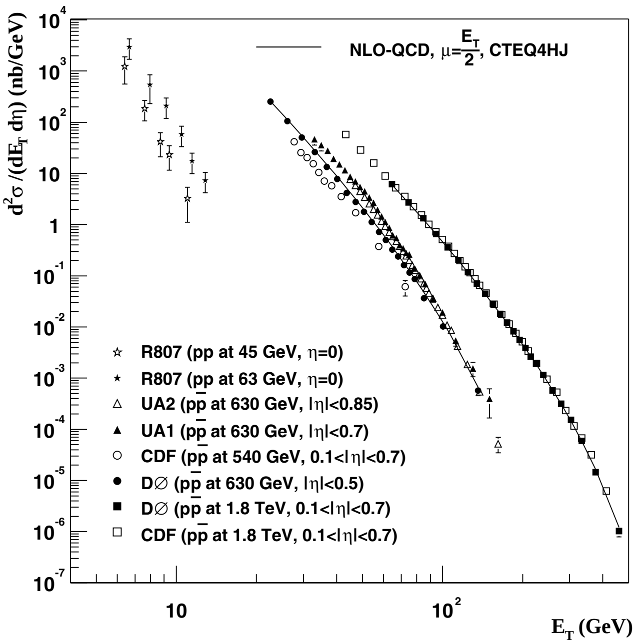

Figure 40.1: Transverse energy dependence of the inclusive differential jet cross sections in the central pseudorapidity region. The error bars are either statistical (DØ), statistical and p_T dependent (UA2), statistical and energy dependent from unsmearing (UA1), uncorrelated (CDF), or total (R806) uncertainties. Comparison of the different experimental results is not straight forward, since the different experiments used different jet reconstruction algorithms. For instance, DØ and CDF used a fixed cone algorithm with a size $\mathcal{R}$=0.7 for all their measurements, compared to a cone size of 1.3 for UA2. **DØ**: Phys. Rev. **D64**, 032003 (2001); **CDF**: Phys. Rev. **D64**, 032001 (2001); **UA1**: Phys. Lett. **B172**, 461 (1986); **UA2**: Phys. Lett. **B257**, 232 (1991); **R807**: Phys. Lett. **B123**, 133 (1983). Next-to-Leading order QCD predictions, using CTEQ4HJ pdfs and $\mu_{R,F} = E_T/2$, are shown for $p\overline{p}$ at 630 GeV and 1.8 TeV. (Courtesy of V.D. Elvira, Fermilab, 2001)

Direct γ Production in $\overline{p}p$ Interactions

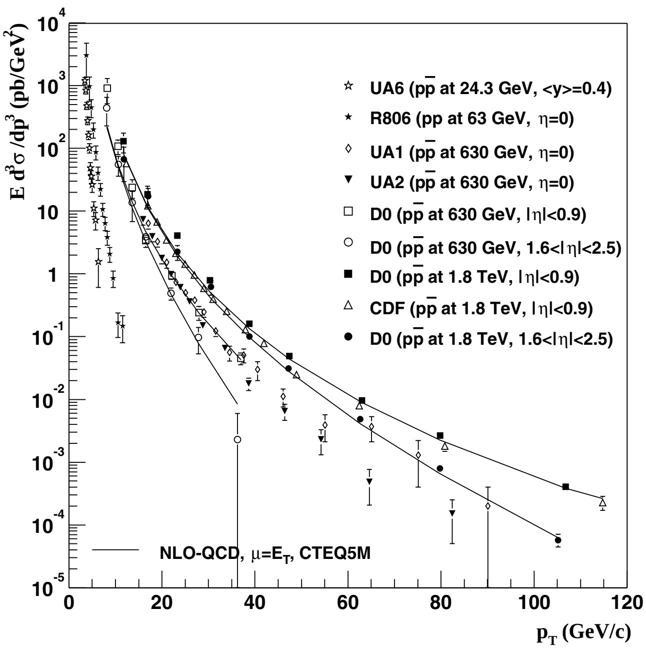

Figure 40.2: Transverse energy dependence of isolated photon cross sections. The error bars are either statistical (CDF), uncorrelated (DØ), or total (UA1, UA2, R806) uncertainties. **DØ**: Phys. Rev. Lett. **87**, 251805 (2001); **CDF**: Phys. Rev. **D73**, 2662 (1994); **UA6**: Phys. Lett. **B206**, 163 (1988); **UA1**: Phys. Lett. **B209**, 385 (1988); **UA2**: Phys. Lett. **B288**, 386 (1992); **R806**: Z. Phys. **C13**, 277 (1982). Next-to-Leading order QCD predictions are shown for $p\overline{p}$ at 630 GeV and 1.8 TeV. (Courtesy of V.D. Elvira, Fermilab, 2001)

Differential Cross Section for W and Z Boson Production

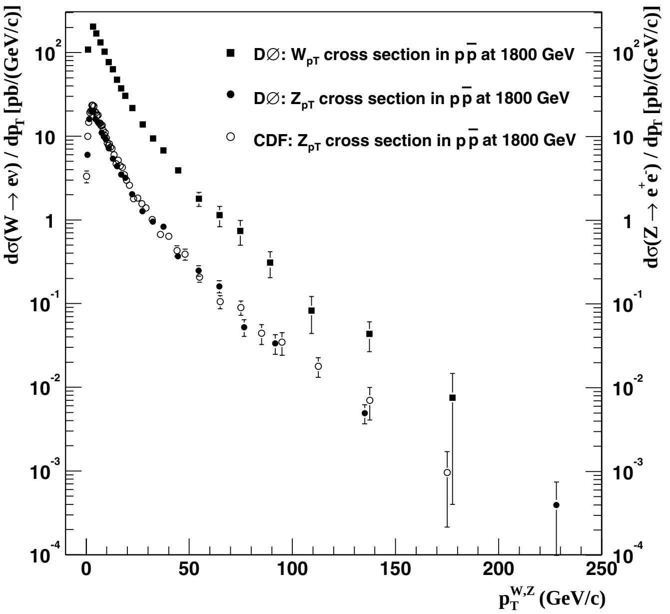

Figure 40.3: Differential cross section for W and Z boson production. The error bars are total errors, excluding the DØ (CDF) 4.4% (3.9%) luminosity uncertainty. **DØ**: Phys. Lett. **B513**, 292 (2001), Phys. Rev. Lett. **84**, 2792 (2000). **CDF**: Phys. Rev. Lett. **84**, 845 (2000). (Courtesy of V.D. Elvira, Fermilab, 2001)

Pseudorapidity Distributions in $\overline{p}p$ Interactions

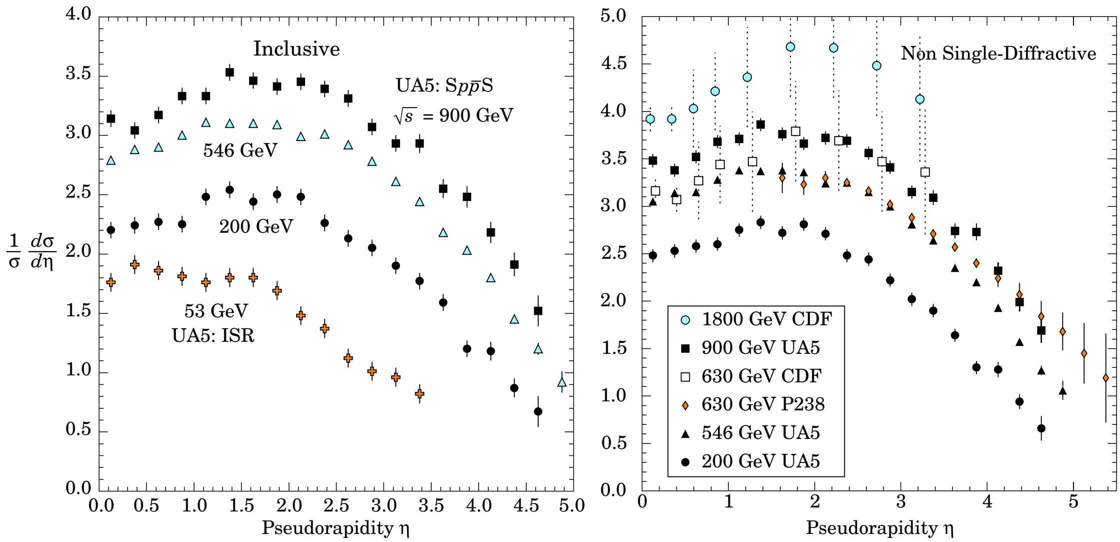

Figure 40.4: Charged particle pseudorapidity distributions in $p\overline{p}$ collisions for 53 GeV $\leq \sqrt{s} \leq$ 1800 GeV. UA5 data from the $Sp\overline{p}S$ are taken from G.J. Alner *et al.*, Z. Phys. **C33**, 1 (1986), and from the ISR from K. Alpgøard *et al.*, Phys. Lett. **112B**, 193 (1982). The UA5 data are shown for both the full inelastic cross-section and with singly diffractive events excluded. Additional non single-diffractive measurements are available from CDF at the Tevatron, F. Abe *et al.*, Phys. Rev. **D41**, 2330 (1990) and Experiment P238 at the $Sp\overline{p}S$, R. Harr *et al.*, Phys. Lett. **B401**, 176 (1997). (Courtesy of D.R. Ward, Cambridge Univ., 1999.)

Average Hadron Multiplicities in Hadronic e^+e^- Annihilation Events

Table 40.1: Average hadron multiplicities per hadronic e^+e^- annihilation event at $\sqrt{s} \approx 10$, 29–35, 91, and 130–200 GeV. The rates given include decay products from resonances with $c\tau < 10$ cm, and include the corresponding anti-particle state. Correlations of the systemaic uncertainties were considered for the calculation of the averages. (Updated July 2003 by O. Biebel, LMU, Munich.)

Particle	$\sqrt{s} \approx 10$ GeV	$\sqrt{s} = 29$–35 GeV	$\sqrt{s} = 91$ GeV	$\sqrt{s} = 130$–200 GeV
Pseudoscalar mesons:				
π^+	6.6 ± 0.2	10.3 ± 0.4	16.99 ± 0.27	21.24 ± 0.39
π^0	3.2 ± 0.3	5.83 ± 0.28	9.42 ± 0.32	
K^+	0.90 ± 0.04	1.48 ± 0.09	2.242 ± 0.063	2.81 ± 0.19
K^0	0.91 ± 0.05	1.48 ± 0.07	2.049 ± 0.026	2.10 ± 0.12
η	0.20 ± 0.04	0.61 ± 0.07	1.049 ± 0.080	
$\eta'(958)$	0.03 ± 0.01	0.26 ± 0.10	0.152 ± 0.020	
D^+	$0.16 \pm 0.03^{(k)}$	0.17 ± 0.03	0.175 ± 0.016	
D^0	$0.37 \pm 0.06^{(k)}$	0.45 ± 0.07	0.454 ± 0.030	
D_s^+	$0.13 \pm 0.02^{(k)}$	$0.45 \pm 0.20^{(a)}$	0.131 ± 0.021	
B^+, B_d^0	—	—	$0.165 \pm 0.026^{(b)}$	
B_s^0	—	—	$0.057 \pm 0.013^{(b)}$	
Scalar mesons:				
$f_0(980)$	0.024 ± 0.006	$0.05 \pm 0.02^{(c)}$	0.146 ± 0.012	
$a_0(980)^\pm$	—	—	$0.27 \pm 0.11^{(d)}$	
Vector mesons:				
$\rho(770)^0$	0.35 ± 0.04	0.81 ± 0.08	1.231 ± 0.098	
$\rho(770)^\pm$	—	—	$2.40 \pm 0.43^{(d)}$	
$\omega(782)$	0.30 ± 0.08	—	1.016 ± 0.065	
$K^*(892)^+$	0.27 ± 0.03	0.64 ± 0.05	0.715 ± 0.059	
$K^*(892)^0$	0.29 ± 0.03	0.56 ± 0.06	0.738 ± 0.024	
$\phi(1020)$	0.044 ± 0.003	0.085 ± 0.011	0.0963 ± 0.0032	
$D^*(2010)^+$	$0.22 \pm 0.04^{(k)}$	0.43 ± 0.07	$0.1937 \pm 0.0057^{(j)}$	
$D^*(2007)^0$	$0.23 \pm 0.06^{(k)}$	0.27 ± 0.11	—	
$D_s^*(2112)^+$	—	—	$0.101 \pm 0.048^{(f)}$	
B^* $^{(g)}$	—	—	0.288 ± 0.026	
$J/\psi(1S)$	$0.00050 \pm 0.00005^{(k)}$	—	$0.0052 \pm 0.0004^{(h)}$	
$\psi(2S)$	—	—	$0.0023 \pm 0.0004^{(h)}$	
$\Upsilon(1S)$	—	—	$0.00014 \pm 0.00007^{(h)}$	
Pseudovector mesons:				
$\chi_{c1}(3510)$	—	—	$0.0041 \pm 0.0011^{(h)}$	
Tensor mesons:				
$f_2(1270)$	0.09 ± 0.02	0.14 ± 0.04	0.166 ± 0.020	
$f_2'(1525)$	—	—	0.012 ± 0.006	
$K_2^*(1430)^+$	—	0.09 ± 0.03	—	
$K_2^*(1430)^0$	—	0.12 ± 0.06	$0.084 \pm 0.022^{(h)}$	
B^{**} $^{(i)}$	—	—	0.118 ± 0.024	
$D_{s1}^\pm$	—	—	$0.0052 \pm 0.0011^{(\ell)}$	
$D_{s2}^{*\pm}$	—	—	$0.0083 \pm 0.0031^{(\ell)}$	
Baryons:				
p	0.253 ± 0.016	0.640 ± 0.050	1.048 ± 0.045	1.41 ± 0.18
Λ	0.080 ± 0.007	0.205 ± 0.010	0.3915 ± 0.0065	0.39 ± 0.03
Σ^0	0.023 ± 0.008	—	0.076 ± 0.011	
Σ^-	—	—	0.081 ± 0.010	
Σ^+	—	—	0.107 ± 0.011	
$\Sigma^\pm$	—	—	0.174 ± 0.009	
Ξ^-	0.0059 ± 0.0007	0.0176 ± 0.0027	0.0258 ± 0.0010	
$\Delta(1232)^{++}$	0.040 ± 0.010	—	0.085 ± 0.014	
$\Sigma(1385)^-$	0.006 ± 0.002	0.017 ± 0.004	0.0240 ± 0.0017	
$\Sigma(1385)^+$	0.005 ± 0.001	0.017 ± 0.004	0.0239 ± 0.0015	
$\Sigma(1385)^\pm$	0.0106 ± 0.0020	0.033 ± 0.008	0.0462 ± 0.0028	
$\Xi(1530)^0$	0.0015 ± 0.0006	—	0.0055 ± 0.0005	
Ω^-	0.0007 ± 0.0004	0.014 ± 0.007	0.0016 ± 0.0003	
Λ_c^+	$0.100 \pm 0.030^{(j)}$	0.110 ± 0.050	0.078 ± 0.017	
Λ_b^0	—	—	0.031 ± 0.016	
$\Sigma_c^{++}, \Sigma_c^0$	0.014 ± 0.007	—	—	
$\Lambda(1520)$	0.008 ± 0.002	—	0.0222 ± 0.0027	

Notes for Table 40.1:

(*a*) B($D_s \to \eta\pi,\ \eta'\pi$) was used (RPP1994).
(*b*) The Standard Model B($Z \to b\overline{b}$) = 0.217 was used.
(*c*) $x_p = p/p_{\rm beam} > 0.1$ only.
(*d*) Both charge states.
(*e*) B($D^*(2010)^+ \to D^0\pi^+$) × B($D^0 \to K^-\pi^+$) has been used (RPP2000).
(*f*) B($D_s^* \to D_S^+\gamma$), B($D_s^+ \to \phi\pi^+$), B($\phi \to K^+K^-$) have been used (RPP1998).
(*g*) Any charge state (*i.e.*, B_d^*, B_u^*, or B_s^*).
(*h*) B($Z \to$ hadrons) = 0.699 was used (RPP1994).
(*i*) Any charge state (*i.e.*, B_d^{**}, B_u^{**}, or B_s^{**}).
(*j*) The value was derived from the cross section of $\Lambda_c^+ \to p\pi K$, assuming the branching fraction to be (3.2 ± 0.7)% (RPP1992).
(*k*) $\sigma_{\rm had} = 3.33 \pm 0.05 \pm 0.21$ nb (**CLEO**: Phys. Rev. **D29**, 1254 (1984)) has been used in converting the measured cross sections to average hadron multiplicities.
(ℓ) Assumes B($D_{s1}^+ \to D^{*+}K^0 + D^{*0}K+$) = 100% and B($D_{s2}^+ \to D^0K^+$) = 45%.

References for Table 40.1:

RPP1992: Phys. Rev. **D45** (1992) and references therein.

RPP1994: Phys. Rev. **D50**, 1173 (1994) and references therein.

RPP1996: Phys. Rev. **D54**, 1 (1996) and references therein.

RPP1998: Eur. Phys. J. **C3**, 1 (1998) and references therein.

RPP2000: Eur. Phys. J. **C15**, 1 (2000) and references therein.

RPP2002: Phys. Rev. **D66**, 010001 (2002) and references therein.

R. Marshall, Rep. Prog. Phys. **52**, 1329 (1989)

A. De Angelis, J. Phys. **G19**, 1233 (1993) and references therein.

ALEPH: D. Buskulic *et al.*: Phys. Lett. **B295**, 396 (1992); Z. Phys. **C64**, 361 (1994); **C69**, 15 (1996); **C69**, 379 (1996); **C73**, 409 (1997); and
R. Barate *et al.*: Z. Phys. **C74**, 451 (1997); Phys. Reports **294**, 1 (1998); Eur. Phys. J. **C5**, 205 (1998); **C16**, 597 (2000); **C16**, 613 (2000); and
A. Heister *et al.*: Phys. Lett. **B526**, 34 (2002); **B528**, 19 (2002).

ARGUS: H. Albrecht *et al.*: Phys. Lett. **230B**, 169 (1989); Z. Phys. **C44**, 547 (1989); **C46**, 15 (1990); **C54**, 1 (1992); **C58**, 199 (1993); **C61**, 1 (1994); Phys. Rep. **276**, 223 (1996).

BaBar: B. Aubert *et al.*: Phys. Rev. Lett. **87**, 162002 (2001).

Belle: K. Abe *et al.*: Phys. Rev. Lett. **88**, 052001 (2002).

CELLO: H.J. Behrend *et al.*: Z. Phys. **C46**, 397 (1990); **C47**, 1 (1990).

CLEO: D. Bortoletto *et al.*, Phys. Rev. **D37**, 1719 (1988).

Crystal Ball: Ch. Bieler *et al.*, Z. Phys. **C49**, 225 (1991).

DELPHI: P. Abreu *et al.*: Z. Phys. **C57**, 181 (1993); **C59**, 533 (1993); **C61**, 40 7(1994); **C65**, 587 (1995); **C67**, 543 (1995); **C68**, 353 (1995); **C73**, 61 (1996); Nucl. Phys. **B444**, 3 (1995); Phys. Lett. **B341**, 109 (1994); **B345**, 598 (1995); **B361**, 207 (1995); **B372**, 172 (1996); **B379**, 309 (1996); **B416**, 233 (1998); **B449**, 364 (1999); **B475**, 429 (2000); Eur. Phys. J. **C6**, 19 (1999); **C5**, 585 (1998); **C18**, 203 (2000).

HRS: S. Abachi *et al.*, Phys. Rev. Lett. **57**, 1990 (1986); and
M. Derrick *et al.*, Phys. Rev. **D35**, 2639 (1987).

L3: M. Acciarri *et al.*: Phys. Lett. **B328**, 223 (1994); **B345**, 589 (1995); **B371**, 126 (1996); **B371**, 137 (1996); **B393**, 465 (1997); **B404**, 390 (1997); **B407**, 351 (1997); **B407**, 389 (1997), erratum ibid. **B427**, 409 (1998); **B453**, 94 (1999); **B479**, 79 (2000).

MARK II: H. Schellman *et al.*, Phys. Rev. **D31**, 3013 (1985); and
G. Wormser *et al.*, Phys. Rev. Lett. **61**, 1057 (1988).

JADE: W. Bartel *et al.*, Z. Phys. **C20**, 187 (1983); andD.D. Pietzl *et al.*, Z. Phys. **C46**, 1 (1990).

OPAL: R. Akers *et al.*: Z. Phys. **C63**, 181 (1994); **C66**, 555 (1995); **C67**, 389 (1995); **C68**, 1 (1995); and
G. Alexander *et al.*: Phys. Lett. **B358**, 162 (1995); Z. Phys. **C70**, 197 (1996); **C72**, 1 (1996); **C72**, 191 (1996); **C73**, 569 (1997); **C73**, 587 (1997); Phys. Lett. **B370**, 185 (1996); and
K. Ackerstaff *et al.*: Z. Phys. **C75**, 192 (1997); Phys. Lett. **B412**, 210 (1997); Eur. Phys. J. **C1**, 439 (1998); **C4**, 19 (1998); **C5**, 1 (1998); **C5**, 411 (1998); and
G. Abbiendi *et al.*: Eur. Phys. J. **C16**, 185 (2000); **C16**, 185 (2000).

PLUTO: Ch. Berger *et al.*, Phys. Lett. **104B**, 79 (1981).

SLD: K. Abe, Phys. Rev. **D59**, 052001 (1999).

TASSO: H. Aihara *et al.*, Z. Phys. **C27**, 27 (1985).

TPC: H. Aihara *et al.*, Phys. Rev. Lett. **53**, 2378 (1984).

Average e^+e^-, pp, and $\overline{p}p$ Multiplicity

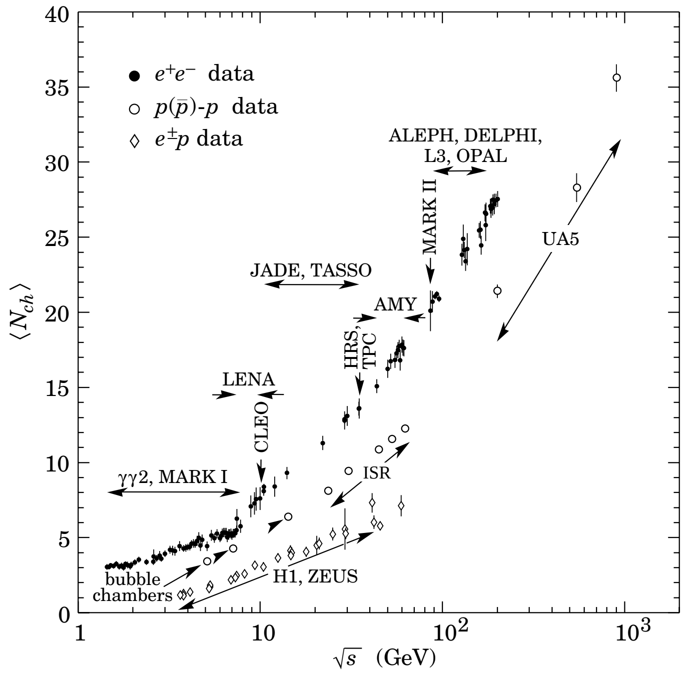

Figure 40.5: Average multiplicity as a function of $\sqrt{s}$ for e^+e^- and $p\overline{p}$ annihilations, and pp and ep collisions. The indicated errors are statistical and systematic errors added in quadrature, except when no systematic errors are given. Files of the data shown in this figure are given in `http://home.cern.ch/b/biebel/www/RPP02`

—

$\boldsymbol{e^+e^-}$: Most e^+e^- measurements include contributions from K^0_S and Λ decays. The $\gamma\gamma 2$ and MARK I measurements contain a systematic 5% error. Points at identical energies have been spread horizontally for clarity:

ALEPH: D. Buskulic *et al.*, Z. Phys. **C69**, 15 (1995); and Z. Phys. **C73**, 409 (1997).

ARGUS: H. Albrecht *et al.*, Z. Phys. **C54**, 13 (1992).

DELPHI: P. Abreu *et al.*, Eur. Phys. J. **C6**, 19 (1999); Phys. Lett. **B372**, 172 (1996); Phys. Lett. **B416**, 233 (1998); and Eur. Phys. J. **C18**, 203 (2000).

L3: M. Acciarri *et al.*, Phys. Lett. **B371**, 137 (1996); Phys. Lett. **B404**, 390 (1997); and Phys. Lett. **B444**, 569 (1998).

OPAL: G. Abbiendi *et al.*, Eur. Phys. J. **C16**, 185 (2000);
K. Ackerstaff *et al.*, Z. Phys. **C75**, 193 (1997);
P.D. Acton *et al.*, Z. Phys. **C53**, 539 (1992) and references therein;
R. Akers *et al.*, Z. Phys. **C68**, 203 (1995).

TOPAZ: K. Nakabayashi *et al.*, Phys. Lett. **B413**, 447 (1997).

VENUS: K. Okabe *et al.*, Phys. Lett. **B423**, 407 (1998).

—

$\boldsymbol{e^{\pm}p}$: Multiplicities have been measured in the current fragmentation region of the Breit frame:

H1: C. Adloff *et al.*, Nucl. Phys. **B504**, 3 (1997).

ZEUS: J. Breitweg *et al.*, Eur. Phys. J. **C11**, 251 (1999);
S. Chekanov *et al.*, Phys. Lett. **B510**, 36 (2001).

—

$\boldsymbol{p^{(\overline{p})}}$: The errors of the $p^{(\overline{p})}$ measurements are the quadratically added statistical and systematic errors, except for the bubble chamber measurements for which only statistical errors are given in the references. The values measured by UA5 exclude single diffractive dissociation:

—

bubble chamber: J. Benecke *et al.*, Nucl. Phys. **B76**, 29 (1976); W.M. Morse *et al.*, Phys. Rev. **D15**, 66 (1977).

ISR: A. Breakstone *et al.*, Phys. Rev. **D30**, 528 (1984).

UA5: G.J. Alner *et al.*, Phys. Lett. **167B**, 476 (1986);
R.E. Ansorge *et al.*, Z. Phys. **C43**, 357 (1989).

(Courtesy of O. Biebel, MPI München, 2001.)

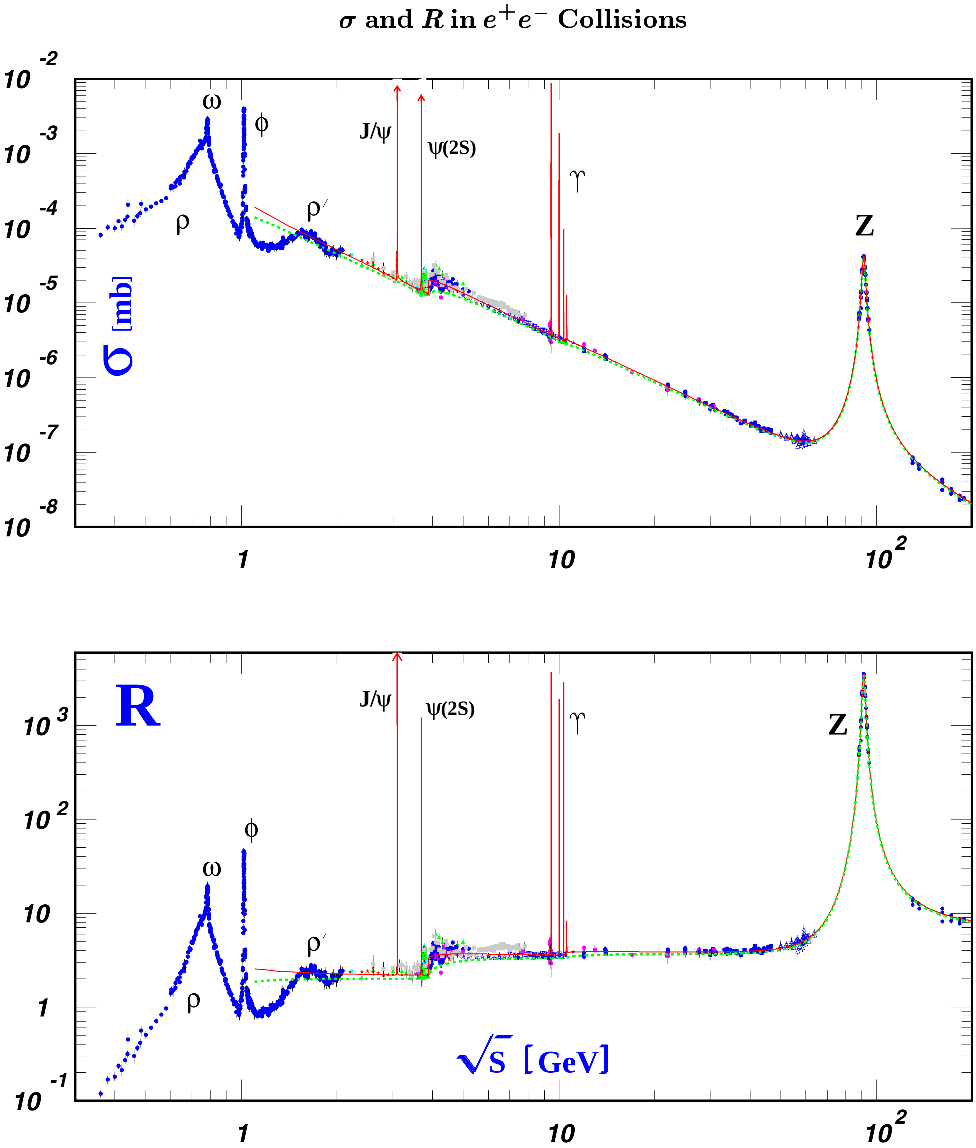

Figure 40.6: World data on the total cross section of $e^+e^- \rightarrow hadrons$ and the ratio $R(s) = \sigma(e^+e^- \rightarrow hadrons, s)/\sigma(e^+e^- \rightarrow \mu^+\mu^-, s)$. $\sigma(e^+e^- \rightarrow hadrons, s)$ is the experimental cross section corrected for initial state radiation and electron-positron vertex loops, $\sigma(e^+e^- \rightarrow \mu^+\mu^-, s) = 4\pi\alpha^2(s)/3s$. Data errors are total below 2 GeV and statistical above 2 GeV. The curves are an educative guide: the broken one is a naive quark-parton model prediction and the solid one is 3-loop pQCD prediction (see "Quantum Chromodynamics" section of this *Review*, Eq. (9.12) or, for more details, K. G. Chetyrkin et al., `hep-ph/0005139`, p.3, Eqs. (1)-(3)). Breit-Wigner parameterizations of J/ψ, $\psi(2S)$, and $\Upsilon(nS), n = 1..4$ are also shown. **Note:** The experimental shapes of these resonances are dominated by machine energy spread and are not shown. The full list of references to the original data and the details of the R ratio extraction from them can be found in `hep-ph/0312114`. Corresponding computer-readable data files are available at `http://pdg.ihep.su/xsect/contents.html`. (Courtesy of the COMPAS(Protvino) and HEPDATA(Durham) Groups, March 2004. Corrections by P. Janot (CERN) and M. Schmitt (Northwestern U.))

R in Light-Flavor, Charm, and Beauty Threshold Regions

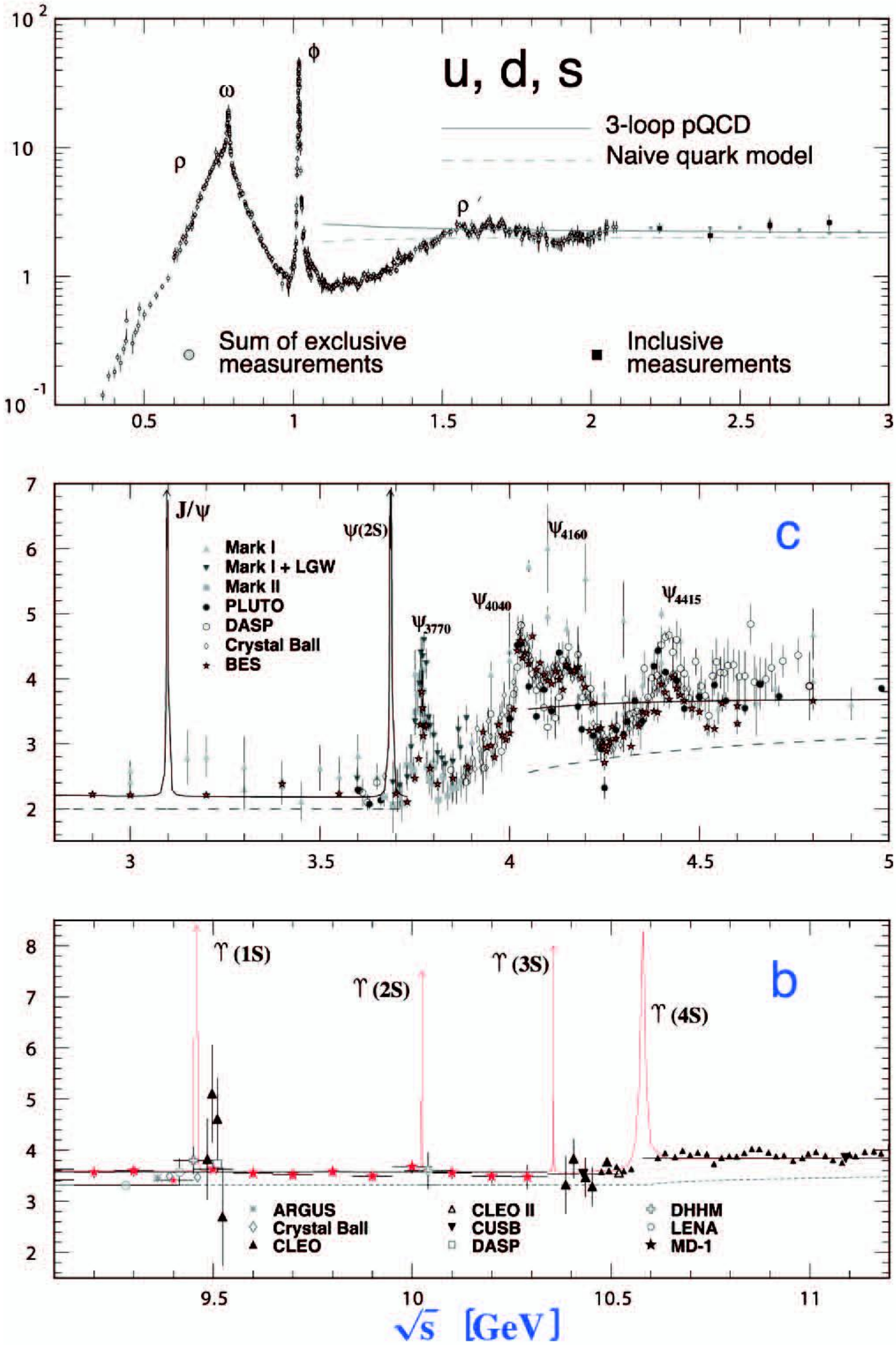

Figure 40.7: R in the light-flavor, charm, and beauty threshold regions. Data errors are total below 2 GeV and statistical above 2 GeV. The curves are the same as in Fig. 40.6. **Note:** CLEO data above $\Upsilon(4S)$ were not fully corrected for radiative effects, and we retain them on the plot only for illustrative purposes with a normalization factor of 0.8. The full list of references to the original data and the details of the R ratio extraction from them can be found in `hep-ph/0312114`. The computer-readable data are available at `http://pdg.ihep.su/xsect/contents.html` (Courtesy of the COMPAS (Protvino) and HEPDATA (Durham) Groups, March 2004.)

Annihilation Cross Section Near M_Z

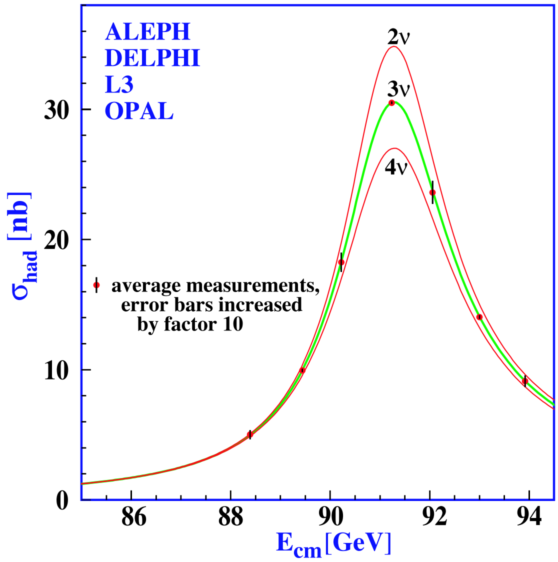

Figure 40.8: Combined data from the ALEPH, DELPHI, L3, and OPAL Collaborations for the cross section in e^+e^- annihilation into hadronic final states as a function of the center-of-mass energy near the Z pole. The curves show the predictions of the Standard Model with two, three, and four species of light neutrinos. The asymmetry of the curve is produced by initial-state radiation. Note that the error bars have been increased by a factor ten for display purposes. References:

ALEPH: R. Barate *et al.*, Eur. Phys. J. **C14**, 1 (2000).
DELPHI: P. Abreu *et al.*, Eur. Phys. J. **C16**, 371 (2000).
L3: M. Acciarri *et al.*, Eur. Phys. J. **C16**, 1 (2000).
OPAL: G. Abbiendi *et al.*, Eur. Phys. J. **C19**, 587 (2001).
Combination: The Four LEP Collaborations (ALEPH, DELPHI, L3, OPAL)
and the Lineshape Sub-group of the LEP Electroweak Working Group, `hep-ph/0101027`.

(Courtesy of M. Grünewald and the LEP Electroweak Working Group, 2003)

Muon Neutrino and Anti-Neutrino Charged-Current Total Cross Section

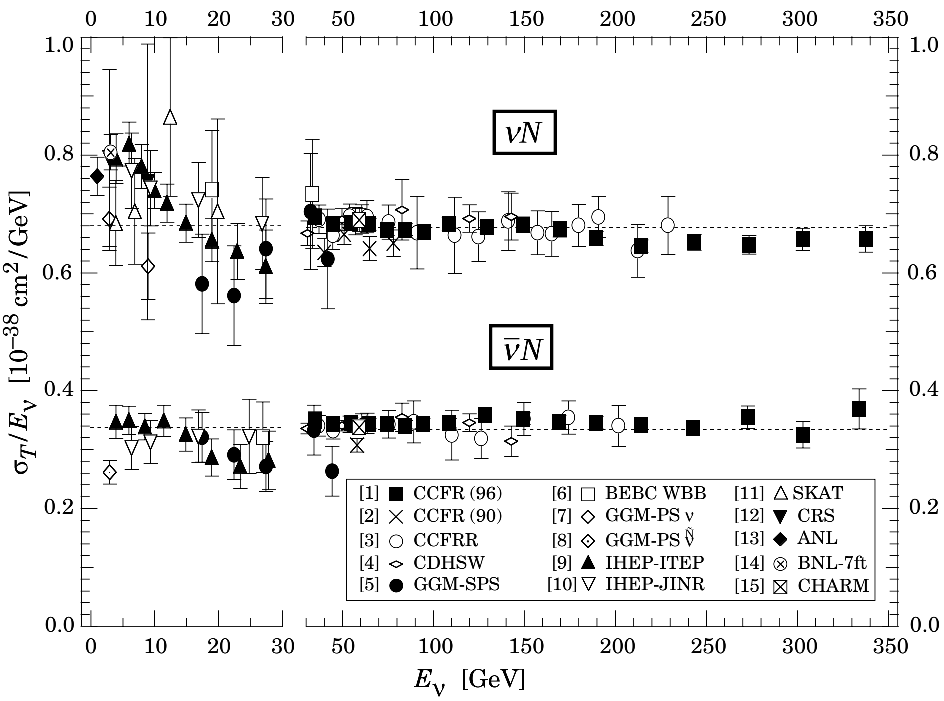

Figure 40.9: σ_T/E_ν, for the muon neutrino and anti-neutrino charged-current total cross section as a function of neutrino energy. The error bars include both statistical and systematic errors. The straight lines are the averaged values over all energies as measured by the experiments in Refs. [1–4]: $= 0.677 \pm 0.014$ $(0.334 \pm 0.008) \times 10^{-38}$ cm^2/GeV. Note the change in the energy scale at 30 GeV. (Courtesy W. Seligman and M.H. Shaevitz, Columbia University, 2001.)

[1] W. Seligman, Ph.D. Thesis, Nevis Report 292 (1996);
[2] P.S. Auchincloss *et al.*, Z. Phys. **C48**, 411 (1990);
[3] D.B. MacFarlane *et al.*, Z. Phys. **C26**, 1 (1984);
[4] P. Berge *et al.*, Z. Phys. **C35**, 443 (1987);
[5] J. Morfin *et al.*, Phys. Lett. **104B**, 235 (1981);
[6] D.C. Colley *et al.*, Z. Phys. **C2**, 187 (1979);
[7] S. Campolillo *et al.*, Phys. Lett. **84B**, 281 (1979);
[8] O. Erriquez *et al.*, Phys. Lett. **80B**, 309 (1979);
[9] V.B. Anikeev *et al.*, Z. Phys. **C70**, 39 (1996);
[10] A.S. Vovenko *et al.*, Sov. J. Nucl. Phys. **30**, 527 (1979);
[11] D.S. Baranov *et al.*, Phys. Lett. **81B**, 255 (1979);
[12] C. Baltay *et al.*, Phys. Rev. Lett. **44**, 916 (1980);
[13] S.J. Barish *et al.*, Phys. Rev. **D19**, 2521 (1979);
[14] N.J. Baker *et al.*, Phys. Rev. **D25**, 617 (1982);
[15] J.V. Allaby *et al.*, Z. Phys. **C38**, 403 (1988).

Table 40.2: Total hadronic cross section. Analytic S-matrix and Regge theory suggest a variety of parameterizations of total cross sections at high energies with different areas of applicability and fits quality.

A ranking procedure, based on measures of different aspects of the quality of the fits to the current evaluated experimental database, allows one to single out the following parameterization of highest rank[1]

$$\sigma^{ab} = Z^{ab} + B\log^2(s/s_0) + Y_1^{ab}(s_1/s)^{\eta_1} - Y_2^{ab}(s_1/s)^{\eta_2}\ , \qquad \sigma^{\overline{a}b} = Z^{ab} + B\log^2(s/s_0) + Y_1^{ab}(s_1/s)^{\eta_1} + Y_2^{ab}(s_1/s)^{\eta_2}$$

where Z^{ab}, B, Y_i^{ab} are in mb, s, s_1, and s_0 are in GeV^2. The scales s_0, s_1, the rate of universal rise of the cross sections B, and exponents η_1 and η_2 are independent of the colliding particles. The scale s_1 is fixed at 1 GeV^2. Terms $Z^{ab} + B\log^2(s/s_0)$ represent the pomerons. The exponents η_1 and η_2 represent lower-lying C-even and C-odd exchanges, respectively. Requiring $\eta_1 = \eta_2$ results in somewhat poorer fits. In addition to total cross sections σ, the measured ratios of the real-to-imaginary parts of the forward scattering amplitudes $\rho = \mathrm{Re}(T)/\mathrm{Im}(T)$ were included in the fits by using s to u crossing symmetry and differential dispersion relations. Global fits were made to the 2003-updated data for $\overline{p}(p)p$, Σ^-p, $\pi^\pm p$, $K^\pm p$, γp, and $\gamma\gamma$ collisions. Exact factorisation hypothesis was used for both Z^{ab} and $\log^2(s/s_0)$ to extend the universal rise of the total hadronic cross sections to the $\gamma p \to hadrons$ and $\gamma\gamma \to hadrons$ collisions. This resulted in reducing the number of adjusted parameters from 21 used for the 2002 edition to 19, and in the higher quality rank of the parameterization. The asymptotic parameters thus obtained were then fixed and used as inputs to a fit to a larger data sample that included cross sections on deuterons (d) and neutrons (n). All fits were produced to data above $\sqrt{s_{\mathrm{min}}} = 5$ GeV.

Fits to $\overline{p}(p)\,p$, Σ^-p, $\pi^\pm p$, $K^\pm p$, γp, $\gamma\gamma$			Beam/	Fits to groups				χ^2/dof
Z	Y_1	Y_2	Target	Z	Y_1	Y_2	B	by groups
35.45(48)	42.53(1.35)	33.34(1.04)	$\overline{p}(p)/p$	35.45(48)	42.53(23)	33.34(33)	0.308(10)	
			$\overline{p}(p)n$	35.80(16)	40.15(1.59)	30.00(96)	0.308(10)	1.029
35.20(1.46)	−199(102)	−264(126)	Σ^-/p	35.20(1.41)	−199(86)	−264(112)	0.308(10)	0.565
20.86(40)	19.24(1.22)	6.03(19)	$\pi^\pm/p$	20.86(3)	19.24(18)	6.03(9)	0.308(10)	0.955
17.91(36)	7.1(1.5)	13.45(40)	$K^\pm/p$	17.91(3)	7.14(25)	13.45(13)	0.308(10)	
			$K^\pm/n$	17.87(6)	5.17(50)	7.23(28)	0.308(10)	0.669
	0.0317(6)		γ/p		0.0320(40)		0.308(10)	
	−0.61(62)E−3		γ/γ		−0.58(61)E−3		0.308(10)	0.766
$\chi^2/dof = 0.971$,	$B = 0.308(10)$ mb,		$\overline{p}(p)/d$	64.35(38)	130(3)	85.5(1.3)	0.537(31)	1.432
$\eta_1 = 0.458(17)$,	$\eta_2 = 0.545(7)$		$\pi^\pm/d$	38.62(21)	59.62(1.53)	1.60(41)	0.461(14)	0.735
$\delta = 0.00308(2)$,	$\sqrt{s_0} = 5.38(50)$ GeV		$K^\pm/d$	33.41(20)	23.66(1.45)	28.70(37)	0.449(14)	0.814

The fitted functions are shown in the following figures, along with one-standard-deviation error bands. When the reduced χ^2 is greater than one, a scale factor has been included to evaluate the parameter values, and to draw the error bands. Where appropriate, statistical and systematic errors were combined quadratically in constructing weights for all fits. On the plots, only statistical error bars are shown. Vertical arrows indicate lower limits on the p_{lab} or E_{cm} range used in the fits.

One can find the details of the global fits (all data on proton target and $\gamma\gamma$ fitted simultaneously) and ranking procedure, as well as the exact parameterizations of the total cross sections, and corresponding ratios of the real to imaginary parts of the forward-scattering amplitudes in the recent paper of COMPETE Collab. [1]. Database used in the fits now includes the recent OPAL and L3 (LEP) $\gamma\gamma$ data, highest energy data for π^-p and Σ^-p from SELEX(FNAL) experiment, $\gamma\,p$ from ZEUS(DESY), cosmic ray $p\,p$ data from the Fly's Eye and AKENO(Agasa), and $\gamma\,p$ data from Baksan experiments. The numerical experimental data were extracted from the PPDS accessible at `http://wwwppds.ihep.su:8001/ppds.html`. Computer-readable data files are also available at `http://pdg.lbl.gov`. (Courtesy of the COMPAS group, IHEP, Protvino, August 2003.) On-line "Predictor" to calculate σ and ρ for any energy from five high rank models is also available at `http://nuclth02.phys.ulg.ac.be/compete/predictor.html/`.

References:

1. J.R. Cudell *et al.* (COMPETE Collab.), Phys. Rev. **D65**, 074024 (2002).
2. G. Abbiendi *et al.* (OPAL Collab.), Eur. Phys. J. **C14**, 199 (2000).
3. M. Acciarri *et al.* (L3 Collab.), Phys. Lett. **B519**, 33 (2001).
4. U. Dersch *et al.* (SELEX Collab.), Nucl. Phys. **B579**, 277 (2000).
5. S. Chekanov *et al.* (ZEUS Collab.), Nucl. Phys. **B627**, 3 (2002).
6. R.M. Baltrusaitis *et al.* (Fly's Eye Collab.), Phys. Rev. Lett. **52**, 1380 (1984).
7. M. Honda *et al.* (Akeno Collab.), Phys. Rev. Lett. **70**, 525 (1993).
8. G.M. Vereshkov*et al.* (Baksan Collab.), Phys. Atom. Nucl. **66**, 565 (2003) [Yad. Fiz. **66**, 591 (2003)].

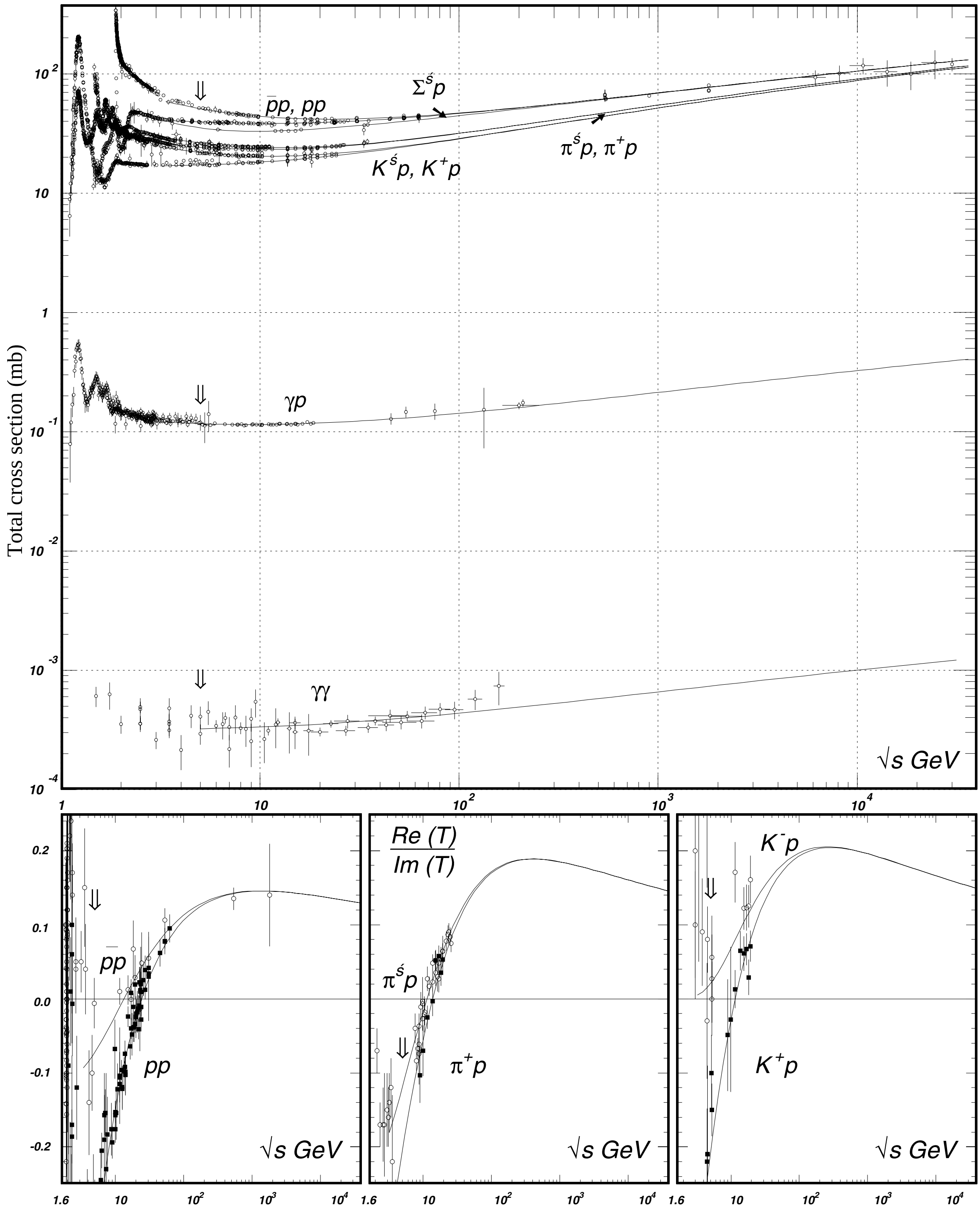

Figure 40.10: Summary of hadronic, γp, and $\gamma\gamma$ total cross sections, and ratio of the real to imaginary parts of the forward hadronic amplitudes. Corresponding computer-readable data files may be found at `http://pdg.lbl.gov/xsect/contents.html`. (Courtesy of the COMPAS group, IHEP, Protvino, August 2003.)

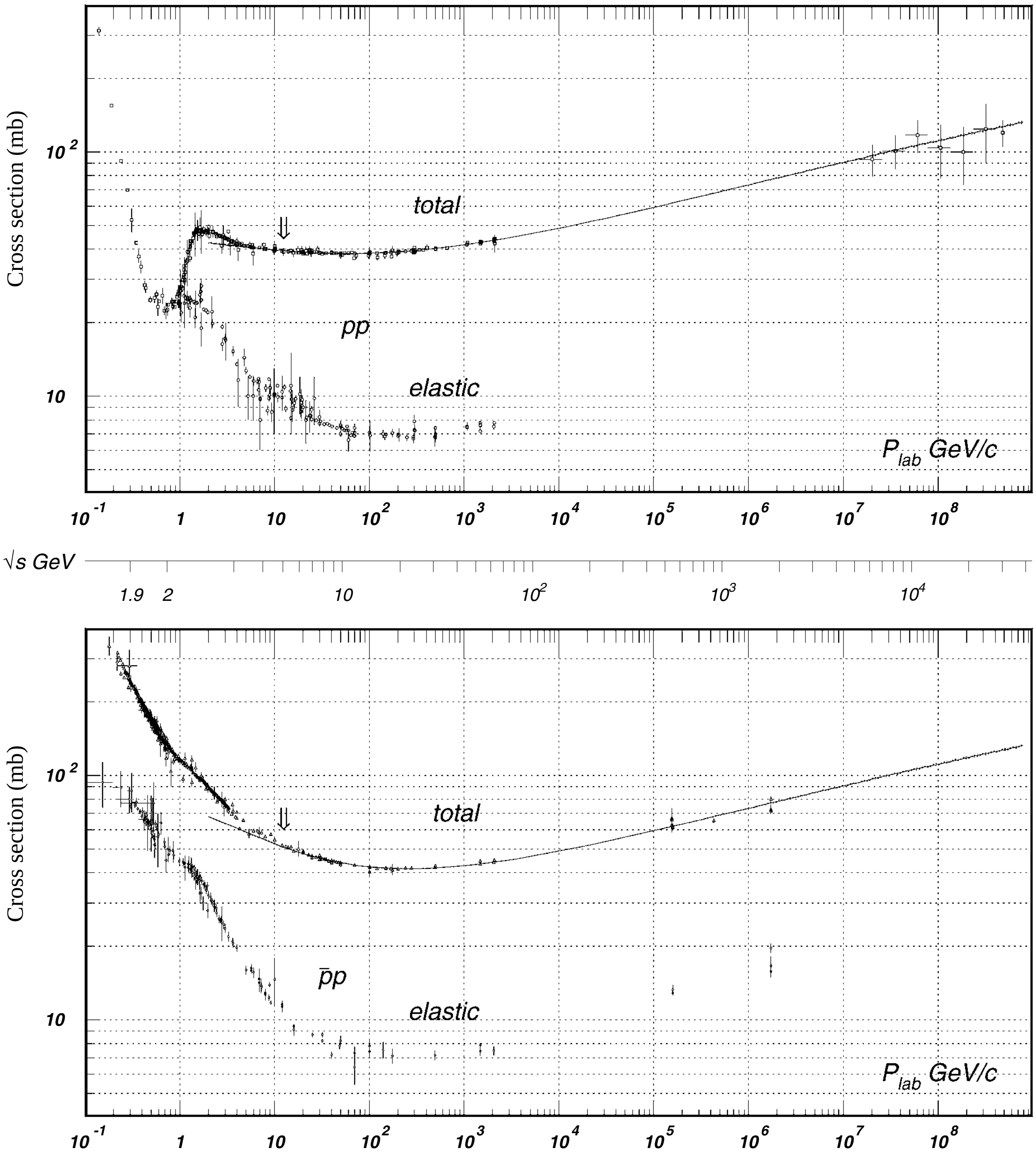

Figure 40.11: Total and elastic cross sections for pp and $\overline{p}p$ collisions as a function of laboratory beam momentum and total center-of-mass energy. Corresponding computer-readable data files may be found at `http://pdg.lbl.gov/xsect/contents.html`. (Courtesy of the COMPAS group, IHEP, Protvino, August 2003.)

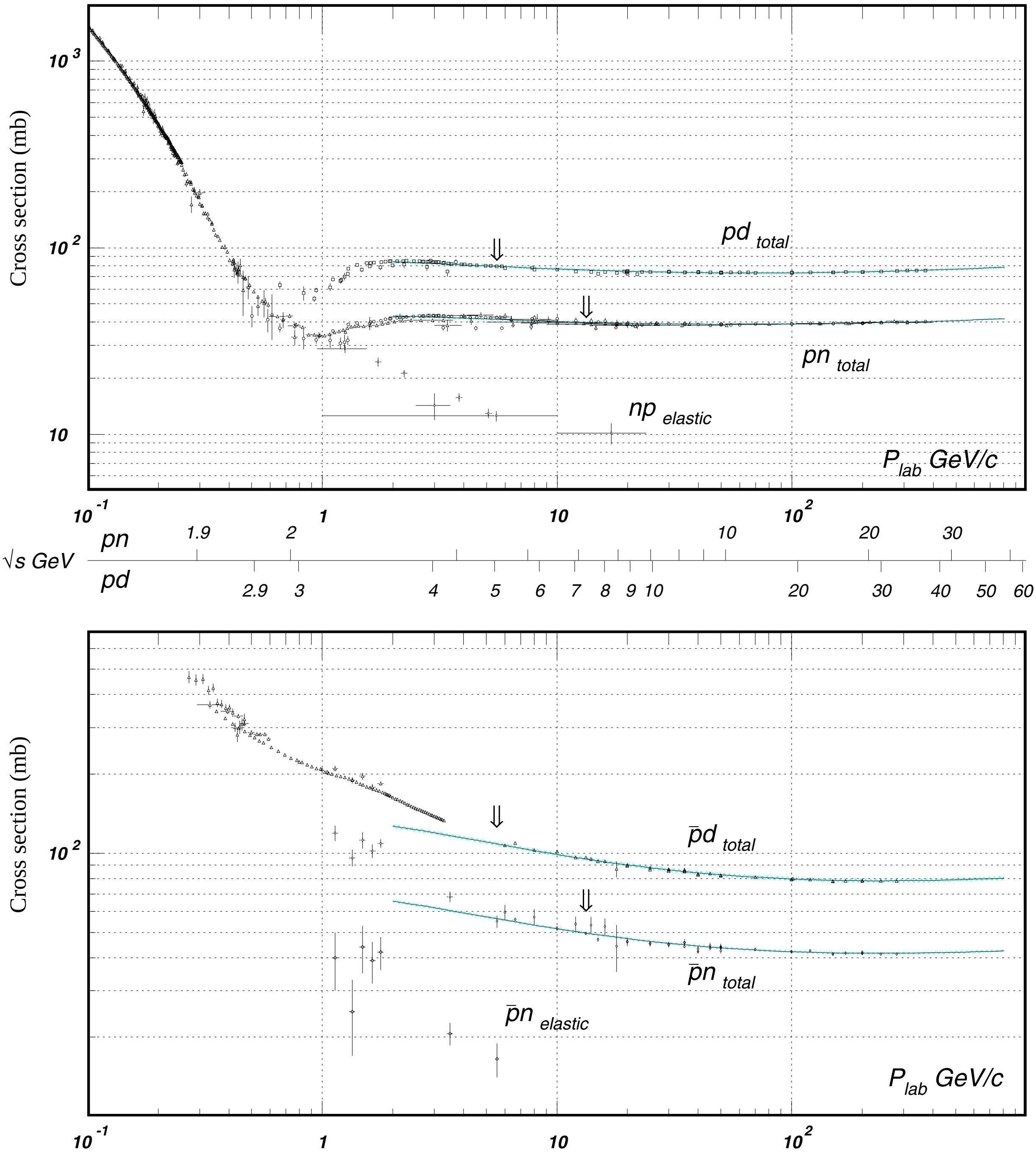

Figure 40.12: Total and elastic cross sections for pd (total only), np, $\overline{p}d$ (total only), and $\overline{p}n$ collisions as a function of laboratory beam momentum and total center-of-mass energy. Corresponding computer-readable data files may be found at `http://pdg.lbl.gov/xsect/contents.html`. (Courtesy of the COMPAS Group, IHEP, Protvino, August 2003.)

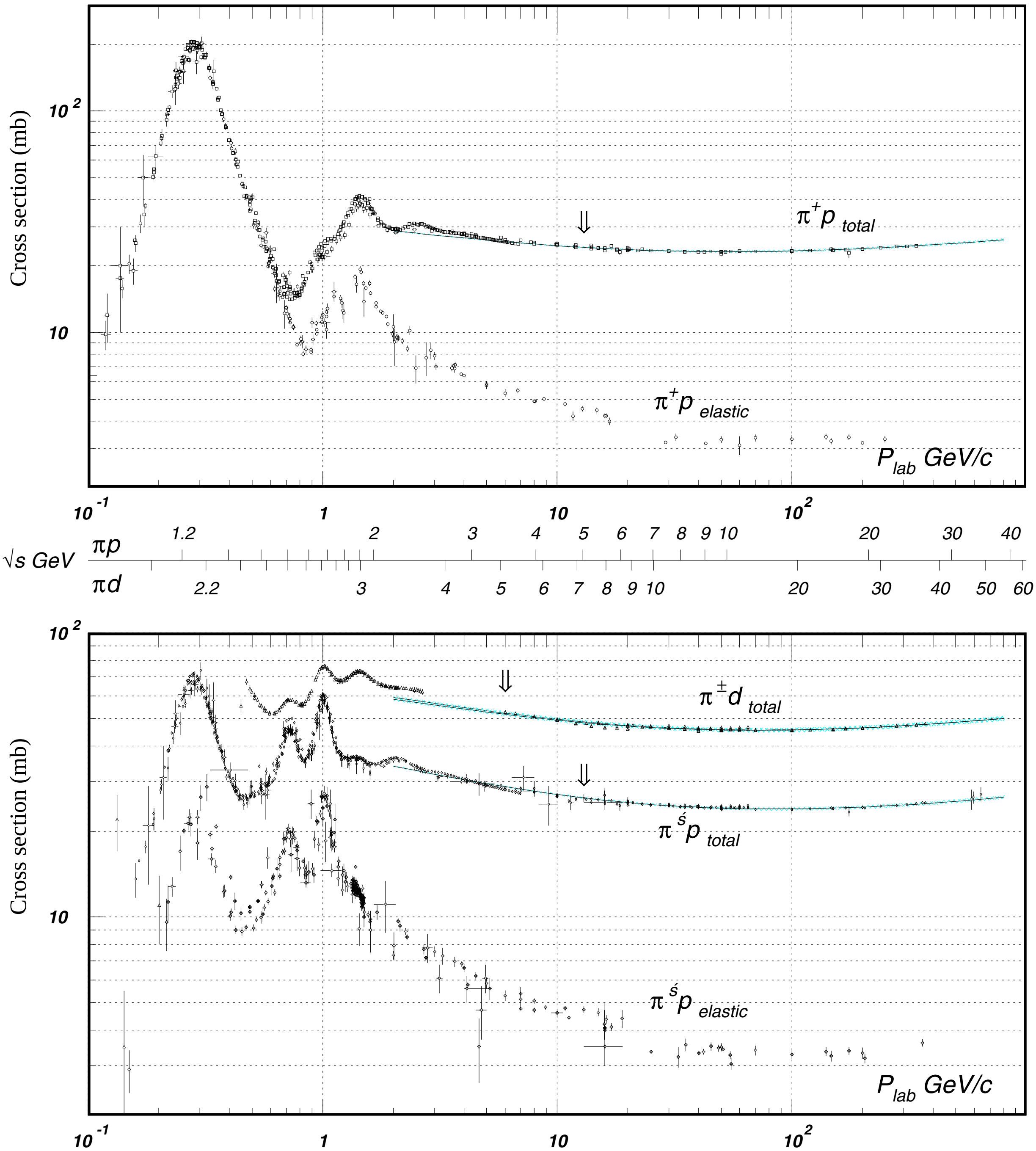

Figure 40.13: Total and elastic cross sections for $\pi^{\pm}p$ and $\pi^{\pm}d$ (total only) collisions as a function of laboratory beam momentum and total center-of-mass energy. Corresponding computer-readable data files may be found at `http://pdg.lbl.gov/xsect/contents.html`. (Courtesy of the COMPAS Group, IHEP, Protvino, August 2003.)

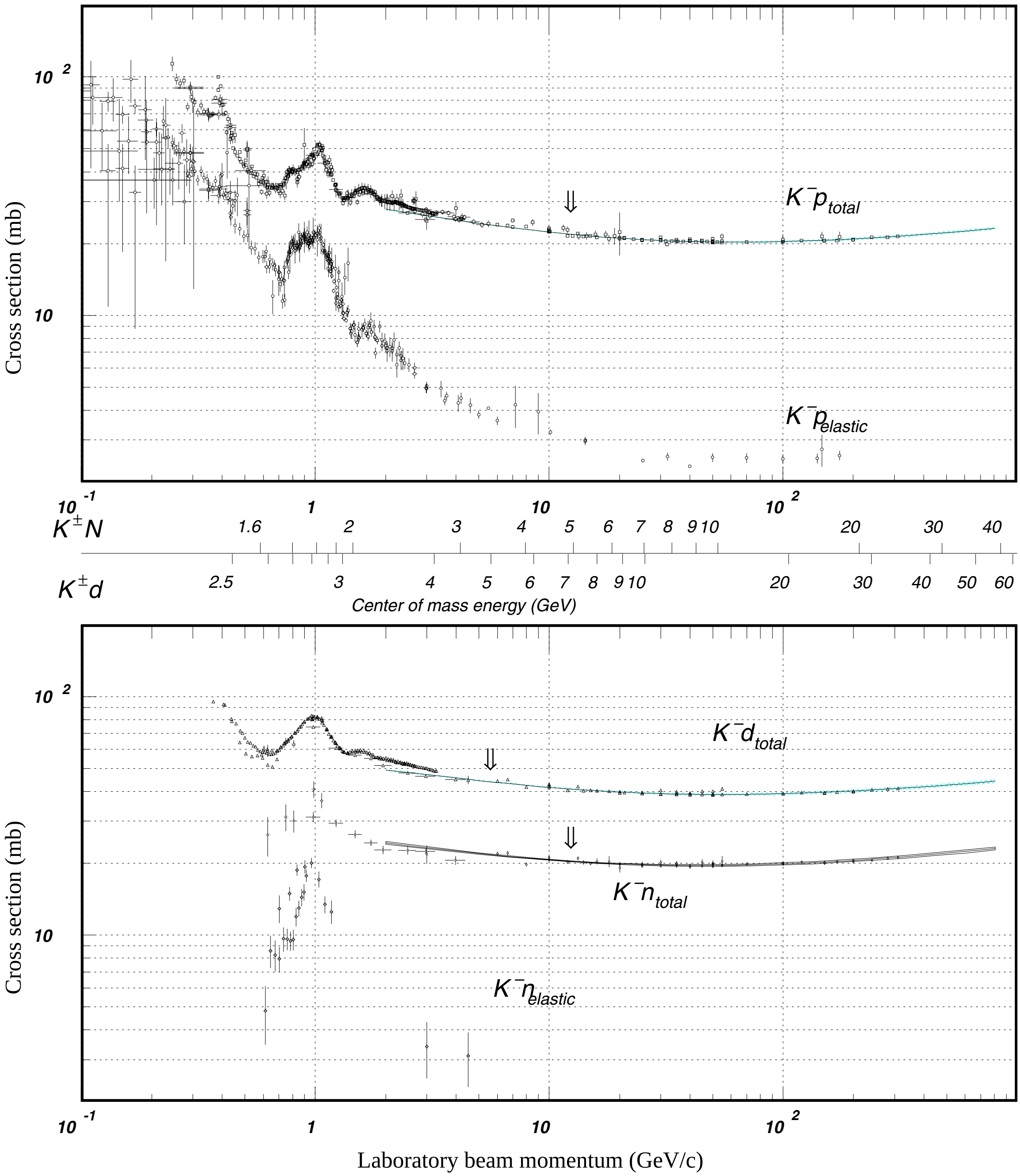

Figure 40.14: Total and elastic cross sections for K^-p and K^-d (total only), and K^-n collisions as a function of laboratory beam momentum and total center-of-mass energy. Corresponding computer-readable data files may be found at `http://pdg.lbl.gov/xsect/contents.html`. (Courtesy of the COMPAS Group, IHEP, Protvino, August 2003.)

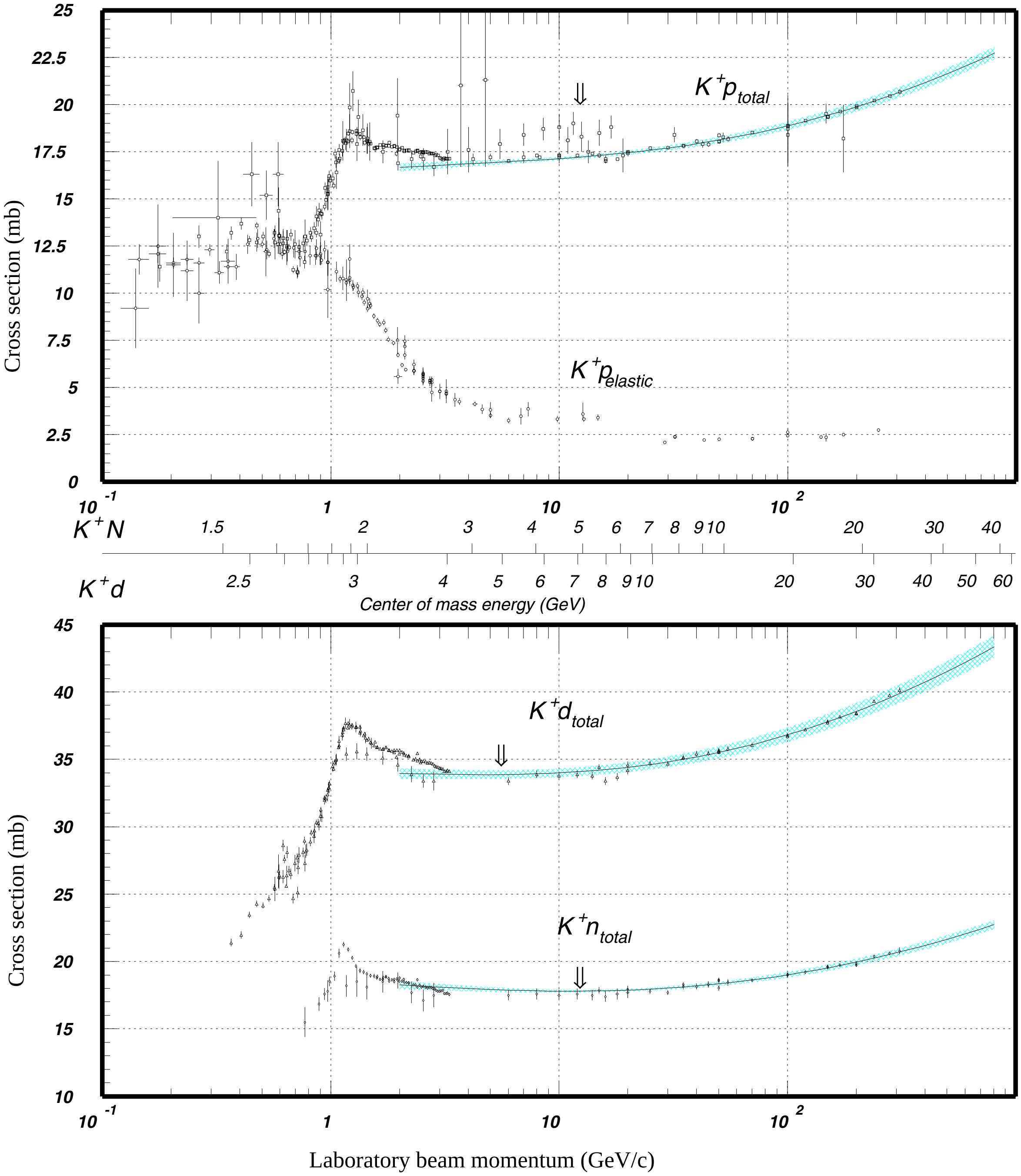

Figure 40.15: Total and elastic cross sections for K^+p and total cross sections for K^+d and K^+n collisions as a function of laboratory beam momentum and total center-of-mass energy. Corresponding computer-readable data files may be found at `http://pdg.lbl.gov/xsect/contents.html`. (Courtesy of the COMPAS Group, IHEP, Protvino, August 2003.)

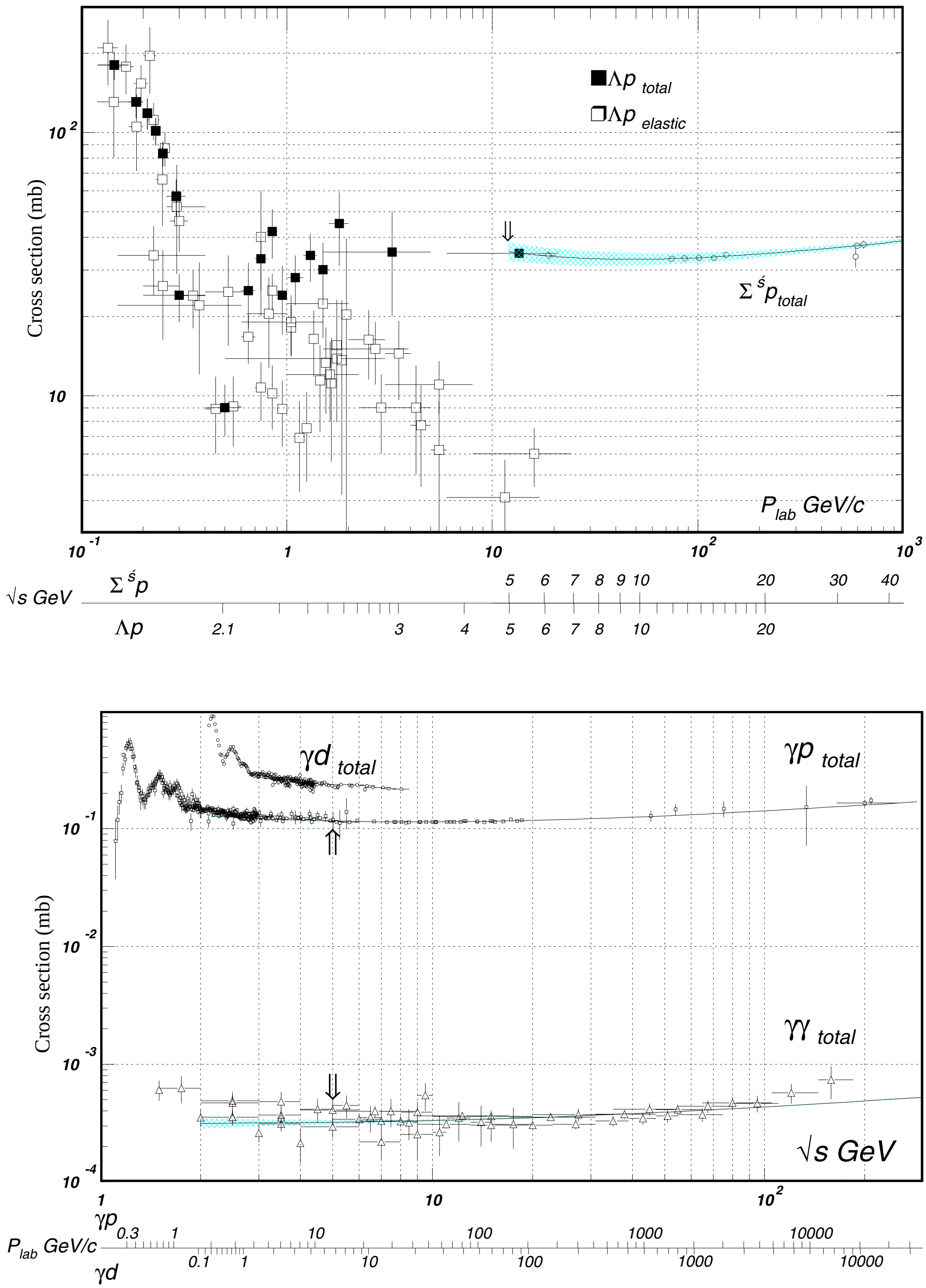

Figure 40.16: Total and elastic cross sections for Λp, total cross section for $\Sigma^- p$, and total hadronic cross sections for γd, γp, and $\gamma\gamma$ collisions as a function of laboratory beam momentum and the total center-of-mass energy. Corresponding computer-readable data files may be found at `http://pdg.lbl.gov/xsect/contents.html`. (Courtesy of the COMPAS group, IHEP, Protvino, August 2003.)